Precision measurement of phase-dependent resonance fluorescence spectra

H. Z. Zhao, Z. H. Lu, A. M. Bacon, L. J. Wang,* and J. E. Thomas
Physics Department, Duke University, Durham, North Carolina 27708-0305
(Received 22 July 1997; revised manuscript received 12 September 1997)

We measure phase-dependent fluorescence spectra for an elementary system: long-lived coherently driven two-level atoms in an atomic beam. Phase-dependent fluorescence spectra measure quadrature noise in the atomic radiation field. These noise spectra are obtained using a homodyne detection scheme that suppresses excess noise by subtracting signals from two identically prepared atomic samples. Noise spectra are obtained for atomic radiation which is in phase (0°) and out of phase (90°) with a resonant driving field, as well as $\pm 45°$ out of phase with an off-resonant driving field. The measured phase-dependent fluorescence spectra are much richer than ordinary fluorescence spectra, and exhibit many novel features. Particularly interesting are phase-dependent noise spectra for off-resonant excitation. These strikingly exhibit direct manifestations of time ordering, which appear as large differences between the measured 45° and $-45°$ quadrature noise spectra. The measured noise spectra are in excellent agreement in magnitude and shape with the results of a quantum treatment using no free parameters. [S1050-2947(98)09002-7]

PACS number(s): 42.50.Lc, 32.80.−t

I. INTRODUCTION

Resonance fluorescence of simple atoms is a central topic in light-matter interactions that has been extensively studied [1]. An atomic beam illuminated by a continuous monochromatic laser field strongly scatters light when the laser is tuned near resonance with a two-level transition. The spectrum of the scattered light observed at right angles to the driving laser beam exhibits a well-known component structure [2], comprising a narrow elastic contribution at the laser frequency and an inelastic triplet structure, where the linewidths are determined by the atomic relaxation rates and the splitting by the Rabi frequency of the driving field [3]. This spectrum has been measured in great detail [4–7], and has been the subject of many theoretical treatments [3,8–19]. Transient fluorescence has been studied for two-level atoms excited by phase-controlled optical fields [20]. In this case, selected dressed states can be excited, leading to fluorescence spectra missing one component [21].

In contrast to fluorescence spectra that are detected without phase sensitivity, *phase-dependent* resonance fluorescence spectra of simple atoms have been relatively unexplored. Phase-dependent resonance fluorescence spectra are obtained by homodyne detection of scattered radiation from free atoms that are irradiated by a quasiresonant field. Phase-dependent resonance fluorescence spectra are much richer than ordinary fluorescence spectra and present many novel features.

In phase-dependent fluorescence experiments, the radiation field $\mathcal{E}$ of the atoms is mixed with a local oscillator (LO) field $|\mathcal{E}_{\rm LO}|e^{i\phi}$ having a controllable fixed phase ϕ relative to the field that drives the atoms. As shown in Sec. II, the atom contribution to the detected power ΔP then is determined by the quadrature operator

$$\hat{x}_\phi(t)=e^{-i\phi}\hat{\mathcal{E}}(t)+e^{i\phi}\hat{\mathcal{E}}^\dagger(t), \tag{1}$$

where $\Delta\hat{P}(t)\propto|\mathcal{E}_{\rm LO}|\hat{x}_\phi(t)$. Fluctuations in the detected power are monitored with a diode detector. A spectrum analyzer is used to obtain the phase-dependent power spectra of the fluctuations in the selected quadrature.

In this paper, we describe precision measurements of phase-dependent fluorescence spectra for long-lived two-level atoms that are driven by a monochromatic laser field. For on-resonance excitation, the in-phase and out-of-phase noise spectra are found to be quite different, and to contain contributions from a variety of atomic noise sources [22]. For off-resonance excitation, pairs of noise spectra for phases of opposite sign are found to display striking differences that arise entirely from time ordering [23]. We show that the relevant time-ordered processes arise from collapses to the ground state following emission of a photon by the coherent part of the atomic dipole moment. A quantum theoretical treatment of the spectra is presented that yields results in excellent quantitative agreement with the data.

Phase-dependent noise power spectra for fluctuations in atomic radiation fields have been studied previously in systems with short radiative lifetimes, with an emphasis on observing quadrature squeezing [24–29]. Phase-dependent noise was observed in the intensity of a probe beam transmitted through sodium vapor in Ref. [26]. The noise spectrum of the transmitted probe field for a pumped, optically thick vapor was studied recently by Kauranen and coworkers [30–32]. This work elucidates the role of pump-probe two-beam coupling in atomic vapors: phase-independent probe noise spectra have been measured to explore two mechanisms which produce excess noise in the transmitted probe intensity. These include direct amplification of vacuum fluctuations in the probe via semiclassical gain and spontaneous scattering of light into the spatial mode of the probe, due to fluctuations in the atomic medium. The latter provides the dominant source of excess probe noise.

Measurements of phase-dependent fluorescence spectra provide insights into the contributions of atomic fluctuations

*Permanent address: NEC Research Institute, 4 Independence Way, Princeton, NJ 08540.

to optical noise spectra. Fluctuations in simple atomic systems play important roles in diverse physical phenomena. They limit the signal-to-background ratio that can be obtained in spectroscopic experiments, and hence limit the accuracy of atomic clocks [24]. In laser cooling and in optical traps, atomic dipole fluctuations cause momentum diffusion, which determines the minimum temperature that can be obtained [33,34]. Atomic fluctuations also limit the amount of squeezing that can be obtained in atomic systems [25–29,35–38]. Despite the many theoretical and experimental studies of noise in radiating atomic systems [39], to our knowledge, detailed measurements of phase-dependent atom noise spectra have not been made previously, and a complete physical picture of the distinct sources of atom noise in atomic radiation fields has not been obtained.

Electromagnetically induced transparency by quantum interference has been demonstrated for eliminating absorption and dispersion in atomic systems [40]. Applications of this method include novel schemes for wave mixing and parametric downconversion, where strong quadrature squeezing may be obtained. Detailed studies of phase-dependent noise in such systems is therefore of interest. This has lead to renewed interest in the theory of phase-dependent fluorescence. Quantum interference in spontaneous emission has been shown to depend on the phase of a driving field that couples the lower levels of an inverted-V three-level system [41]. The role of initial coherence in harmonic generation in two-level systems also has been explored [42].

Recently, the phase-dependent spectrum of light scattered from Bose condensates in two different atomic states has been calculated. It is predicted to be a direct probe of the relative phase of the condensates [43]. Hence, detailed studies of phase-dependent fluorescence for simple atomic systems continue to be of fundamental interest.

Our measurements of phase-dependent resonance fluorescence spectra are obtained using a homodyne detection scheme that suppresses excess noise by subtracting signals from two identically prepared atomic samples [22,23]. We use atoms with a radiative lifetime long compared to the transit time of the atoms across the driving laser fields, so that noise power spectra can be analyzed in terms of a simple fluctuating Bloch vector picture. As mentioned above, very different noise spectra are measured for radiation which is in phase or out of phase with a resonant driving field. These noise spectra are found to be in good qualitative agreement with previous predictions of phase-dependent noise in the resonance fluorescence of a driven atomic system with a short radiative lifetime [35]. As shown below, the data are in excellent quantitative agreement with a quantum treatment for a long-lived system.

Particularly interesting is the striking appearance of the effects of time ordering in the phase-dependent fluorescence spectra for off-resonant excitation. Previously, using correlation methods and frequency-filtered resonance fluorescence, it has been possible to observe temporal correlations between sideband photons [44] and interference between different time orderings of Rayleigh and sideband photons [45]. In the present measurements, quadrature power spectra for plus or minus 45° phases are found to be markedly different when the driving field is off resonance. This difference is shown to be a direct manifestation of time ordering [23] as described physically in Sec. II, and in more detail in Sec. V.

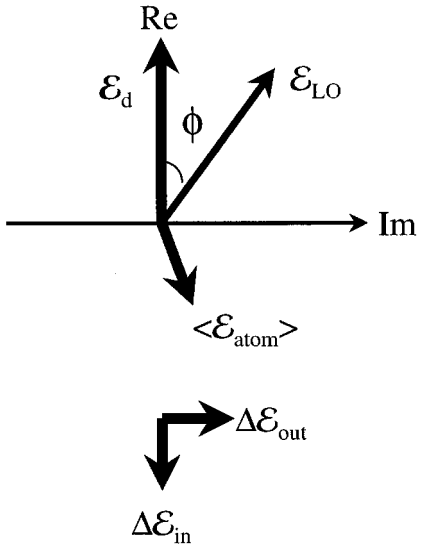

FIG. 1. Measurement of atomic radiation noise via phase-dependent fluorescence spectra. The amplitudes of the driving field $\mathcal{E}_d$, the local oscillator field $\mathcal{E}_{LO}$, and the atom field $\langle\mathcal{E}_{atom}\rangle+\Delta\mathcal{E}_{in}+i\Delta\mathcal{E}_{out}$ are plotted as phasors.

The remainder of this paper is organized as follows. Section II provides a brief physical description of phase-dependent resonance fluorescence. It is shown that a classical description fails to predict the measured spectra. Some of the issues raised in interpreting the noise spectra are described including the origin of the observed time ordering effects. Section III describes the experimental system. We discuss the suppression of excess noise in homodyne detection by subtracting signals from two identically prepared atomic samples. This is treated in detail in Appendix A. In Sec. IV the measured phase-dependent resonance fluorescence spectra are presented. Section V summarizes the results of the quantum theory of the phase-dependent resonance fluorescence spectra for long-lived atoms. In order to obtain predictions that can be quantitatively compared both in magnitude and in shape with the data, a detailed treatment is given in Appendix B. Concluding remarks are given in Sec. VI.

II. PHYSICAL PICTURE OF PHASE-DEPENDENT FLUORESCENCE

As described in Sec. I, phase-dependent resonance fluorescence spectra are obtained by homodyne detection of scattered radiation from free atoms that are irradiated by a quasiresonant driving field. Figure 1 depicts the measurement of phase-dependent noise in the atom radiation field via phase-dependent fluorescence. The field components shown in the figure are slowly varying amplitudes plotted as phasors, with a common optical phase factor $e^{-i\Omega t}$ removed. Here Ω is the frequency for both the local oscillator and the driving field. Without loss of generality, the driving field amplitude $\mathcal{E}_d$ is taken to be real.

In response to the driving field, the atom radiates a mean field $\langle\mathcal{E}_{atom}\rangle$. For resonant excitation of an atom that is initially in the ground state, the mean field of the atom will be 180° out of phase with the driving field in the forward-

scattering direction. This causes absorption of the driving field. In addition to the mean field, the atomic radiation field contains fluctuating components. In general, there will be a fluctuating component in phase with the driving field, $\Delta\mathcal{E}_{\rm in}$, and a fluctuating component 90° out of phase with the driving field, $\Delta\mathcal{E}_{\rm out}$. The net radiation field of the atom can be written in the form

$$\mathcal{E}(t)=\langle\mathcal{E}_{\rm atom}\rangle+\Delta\mathcal{E}_{\rm in}+i\Delta\mathcal{E}_{\rm out}. \tag{2}$$

To measure the fluctuations, the atomic radiation field is mixed with a strong (LO) field $\mathcal{E}_{\rm LO}$ at a diode detector. In the measurements, the relative (classical) phase ϕ between the strong LO field and the strong driving field is fixed and adjustable. The detector measures the total power of the combined field, $\propto|\mathcal{E}_{\rm LO}+\mathcal{E}|^2$. The dominant atom contribution to the fluctuation in the detected power arises from the interference terms

$$\Delta P(t)\propto\mathcal{E}_{\rm LO}^{*}\mathcal{E}(t)+\text{c.c.} \tag{3}$$

Since $\mathcal{E}_{\rm LO}=|\mathcal{E}_{\rm LO}|e^{i\phi}$, the atom contribution to the detected power fluctuation can be written as

$$\Delta\hat{P}(t)\propto|\mathcal{E}_{\rm LO}|\hat{x}_{\phi}(t), \tag{4}$$

where $\hat{x}_{\phi}(t)$ is the quadrature operator,

$$\hat{x}_{\phi}(t)=e^{-i\phi}\hat{\mathcal{E}}(t)+e^{i\phi}\hat{\mathcal{E}}^{\dagger}(t). \tag{5}$$

For a strong classical LO field, small fluctuations in the radiation field of single atoms are converted into large detectable power fluctuations.

The spectrum of the power fluctuations is measured with a spectrum analyzer that yields a one-sided power spectrum proportional to the Fourier transform of the autocorrelation function of the power fluctuations:

$$S_{\phi}(\omega)=\frac{2}{\pi}\int_0^{\infty}d\tau\,\cos\omega\tau\langle\Delta\hat{P}(t)\Delta\hat{P}(t+\tau)\rangle$$

$$\propto\frac{2}{\pi}\int_0^{\infty}d\tau\,\cos\omega\tau\langle\hat{x}_{\phi}(t)\hat{x}_{\phi}(t+\tau)\rangle. \tag{6}$$

Here ω is the spectrum analyzer frequency. The angled brackets denote a quantum statistical average and a time average over t.

In the experiments described below, the interaction time of the atoms with the laser fields is determined by the transit time of the atoms to cross the driving field region. The LO is spatially matched to the driving field, so that the time to cross the observation region is identical to the transit time to cross the driving beam. For simplicity in the following discussion, we have left out the factor that describes the finite transit time in the integrands of Eq. (6). This factor determines the transit time limited spectral width of the various components of the noise power spectrum, and is included in the more complete quantum theory described in Sec. V.

When the relative phase ϕ is set to 0°, the LO is in phase with the driving field, and atom-field fluctuations in phase with the driving field are detected. Measurement of the power spectrum in this case is equivalent to measuring the noise in the transmitted power of the driving field alone. With the LO relative phase set to $\phi=90°$, fluctuations out of phase with the driving field are detected. In this case, when the driving field frequency is resonant, the LO is 90° out of phase with the mean radiation field of the sample. The mean power measured at the detector then is the same whether the atoms are present or not. Nevertheless, a nonzero noise power spectrum is observed experimentally for $\phi=90°$. Finally, with $\phi=\pm45°$, the noise power spectrum depends on the cross correlation between atom-field fluctuations that are in phase and out of phase with the driving field.

An important point is that for optically thin samples of atoms, the correlation function that appears in Eq. (6) contains only the independent contributions of *single* atoms [37]. This arises because the atoms enter the interaction region at random times and are uncorrelated with one another. Hence the mean-square noise is the sum of the mean-square noise contributions from each of the N atoms that are in the interaction region.

It is interesting to try to interpret the measured phase-dependent noise power spectra by treating the atoms as classical dipoles emitting a radiation field equal to the mean field of a coherently driven two-level atom. The classical calculation fails in a number of interesting ways, as described below.

The classical power change arises from the interference between the LO field and the *mean* field of a single long-lived two-level atom. For an atom that enters the driving beam in its ground state at time $t=0$, the power change takes the form

$$\langle\Delta\hat{P}(t)\rangle\propto\frac{\beta_d}{\beta'}\frac{\sin\theta}{2}\cos\phi+\frac{\beta_d\Delta}{\beta'^2}\frac{1-\cos\theta}{2}\sin\phi. \tag{7}$$

Here $\beta_d=\mu|\mathcal{E}_d|/\hbar$ is the Rabi frequency arising from the driving field, and Δ is the detuning of the driving/LO fields from atomic resonance. β' is the generalized Rabi frequency, $\beta'\equiv\sqrt{\beta_d^2+\Delta^2}$. For a driving beam with a square profile where β_d is constant, the angle $\theta=\beta' t$. Here $0\leqslant t\leqslant\tau_o$, with τ_o the interaction (transit) time for atoms to cross the driving/LO beams. Equation (7) describes the coherent radiation of a two-level atom, neglecting spontaneous emission. This is appropriate in our experiments, for which the interaction (transit) time is short compared to the spontaneous lifetime. Note that we have left out multiplicative factors that include the LO field magnitude. These factors determine the transit-time-limited bandwidth, as discussed above.

Classical noise power spectra are determined from Eq. (6) using Eq. (7). In doing this, we are treating the atomic radiators as though they are unaffected by the radiation process. The results of this calculation are shown in Fig. 2 for on-resonance excitation with $\phi=0°$ and 90°, and for off-resonance excitation with $\phi=\pm45°$ (or $\phi=180\pm45°$). To compare the classical results to the data properly, the plots are calculated using the same methods and the same parameters (Rabi frequency, detuning, atom density, etc.) as for the exact quantum theory results of Sec. V, but retaining only the classical contributions that correspond to Eq. (7).

One immediately sees that the classical calculation of Fig. 2 is in poor agreement with the data shown in Figs. 6, 7, and

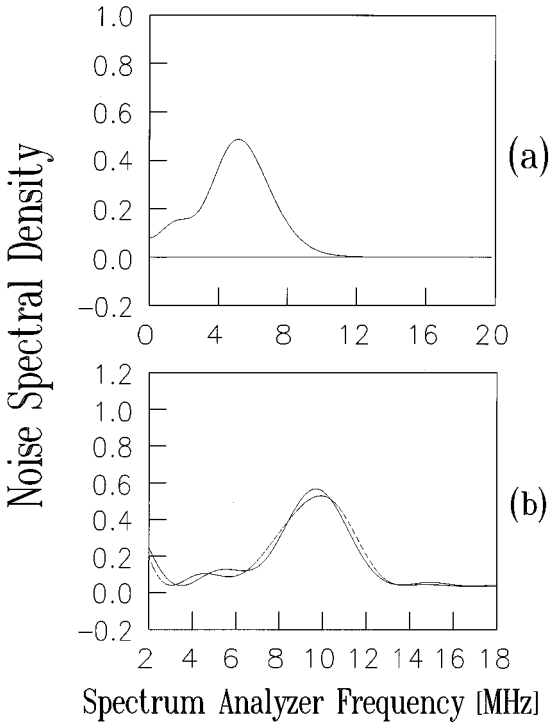

FIG. 2. Classical calculation of phase-dependent fluorescence spectra showing poor agreement with the measurements of Figs. 6, 7, and 8. (a) On-resonance in-phase $\phi=0$ spectrum (peak) and out-of-phase $\phi=90°$ spectrum (horizontal line). (b) Off-resonance spectrum for $\phi=135°$ (solid line) and $\phi=225°$ (dashed line).

8. It also disagrees with the corresponding quantum calculations shown in the same figures. The classical calculation of the on-resonance $\phi=0°$ noise spectrum displays a peak at the generalized Rabi frequency. Classically, this arises solely from the modulation of the coherent dipole moment at the generalized Rabi frequency as the atoms cross the driving field. While the location of the peak is correct, the calculated magnitude is smaller than that measured in the experiments and predicted by the quantum theory.

The classical theory also predicts no noise for the on-resonance $\phi=90°$ power spectrum, since the LO is out of phase with the atom radiation field, and experiences no power change as the atoms traverse the driving beam. By contrast, the measured power spectrum is nonzero, and consists of a large noise peak centered at the origin.

Finally, for $\phi=\pm45°$ and off-resonance excitation, the classical theory predicts essentially identical noise spectra at frequencies near the generalized Rabi frequency. By contrast, the measured spectra for $\phi=\pm45°$ differ dramatically in this frequency region, and the noise peaks are considerably larger than those predicted classically.

Both the data and the quantum theory exhibit squeezing at certain frequencies, where the total noise dips below the shot-noise level, i.e, below the zero level in Fig. 8. By contrast, the classical noise power spectrum can be written as the magnitude squared of the Fourier transform of the classical power change of Eq. (7). Hence the classical noise power spectrum is always positive definite, and will never exhibit squeezing.

The classical theory fails in part because the atomic radiation field contains both coherent contributions from the expectation value of the dipole operator (as used in the classical calculation), and contributions that exhibit quantum fluctuations [14] that are neglected in the classical calculation. Spontaneous emission into the LO mode from both the coherent and fluctuating parts of the dipole occurs with similar rates. Since the spontaneous field of the atom has a random phase component, even with the LO phase set at 90° to the driving field, there will be noise in the detected power and hence a nonzero noise power spectrum.

The appearance of noise in the $\phi=90°$ quadrature shows that phase-dependent fluorescence measurement can distinguish incoherent spontaneous emission in the presence of coherent emission. The latter is out of phase with the LO for $\phi=90°$ with resonant excitation, and hence causes no fluctuations. By contrast, in ordinary resonance fluorescence measurement, the two contributions are inseparable.

Fluctuations in the atomic dipole moment are phase dependent, and can be described in terms of fluctuations in the atomic pseudospin (Bloch vector) operators [22]. When the Bloch vector is rotated so that it lies along a given quadrature axis, the fluctuations along that axis are suppressed, since the length of the Bloch vector is conserved. A heuristic picture of the noise spectra in terms of phase-dependent and phase-independent components of the Bloch vector projection noise was given in Ref. [22]. The phase-dependent part of the projection noise spectrum can make a negative contribution to the total noise, that tends to cause squeezing, i.e., the field noise can be suppressed as discussed above. However, the phase-independent part of the Bloch vector noise spectrum can exhibit increased noise at the same frequency. Hence the total noise need not exhibit squeezing. As noted in Ref. [22], separation of the atom noise contributions is somewhat artificial, since only certain combinations of these noise terms can be isolated in the experiments.

The classical theory also fails to incorporate the effects of time ordering [23]. A formal description of the effects of time ordering is given in Ref. [23], where it is shown that for off-resonant excitation, the difference between the $\pm45°$ spectra arises entirely from the fundamental noncommutativity of two positive frequency source field operators evaluated at different times. Time ordering arises in multiple time measurements because the first measurement alters the quantum state of the atom, and therefore affects the second measurement. The correlation function of the quadrature operator appearing in Eq. (6) involves a two-time field measurement, and hence should incorporate time ordering effects.

A physical picture of the origin of the effects of time ordering in the $\pm45°$ phase-dependent fluorescence spectra can be obtained for atoms with a long radiative lifetime, as used in the experiments. The time-ordered contributions that cause the striking difference between these spectra can be interpreted as arising entirely from the coherent part of the dipole moment. However, we cannot treat the atom as a classical radiator: we must incorporate collapses to the ground state following detection of a fluctuation arising from photoemission by the atom [14], as we now show.

Equation (6) shows that the noise power spectrum depends on the two-time power autocorrelation function. Fluctuations in the detected power at times t and $t+\tau$ for $\tau\geqslant0$ determine the correlation function. These fluctuations arise from the interference between the LO field and the radiation

field of single atoms. Photons radiated by the atom can arise from either the coherent part of the atomic dipole moment, or by spontaneous emission from the excited state. We consider first the coherent dipole.

Suppose we detect a power fluctuation at time t arising from photon emitted by the coherent part of the atomic dipole. This fluctuation is $\langle \Delta \hat{P}(t) \rangle$, as given by Eq. (7). Immediately following detection of a fluctuation at time t, the atom is reduced to the ground state. A second correlated fluctuation arises from the coherent dipole of the same atom at time $t' = t + \tau$, since this atom is known to be in the ground state at time t. This power fluctuation is just $\langle \Delta \hat{P}(t' - t) \rangle$, where $t' - t = \tau$. The correlation function is determined by the product $\propto \langle \Delta \hat{P}(t) \rangle \langle \Delta \hat{P}(t' - t) \rangle$. For long-lived atoms, we need not be concerned with spontaneous emission between the times t and t'.

Equation (7) shows that phase-dependent terms appear in the product $\langle \Delta \hat{P}(t) \rangle \langle \Delta \hat{P}(t' - t) \rangle$. These are proportional to $\cos^2\phi$, $\sin^2\phi$, and $\sin 2\phi$. The first two terms contribute identically to both the plus and minus 45° noise spectra. However, the last term changes sign and causes the $\pm 45°$ noise spectra given by Eq. (6) to differ. This term arises from the cross correlation between absorptive and dispersive contributions to the detected power, i.e., from the cross correlation between fluctuations in phase and out of phase with the driving field.

It is instructive to look closely at this cross-correlation term that is proportional to $\sin 2\phi$. With the definitions $\theta \equiv \beta' t$ and $\theta' = \beta' t'$, Eq. (7) shows that the cross correlation is proportional to the detuning, and takes the form

$$\frac{\beta_d^2 \Delta}{2\beta'^3} \left[\frac{\sin\theta}{2} \frac{1 - \cos(\theta' - \theta)}{2} + \frac{(1 - \cos\theta)}{2} \frac{\sin(\theta' - \theta)}{2} \right] \sin 2\phi. \tag{8}$$

The first term in Eq. (8) corresponds to detection of a fluctuation at time t arising from the coherent dipole moment that is in phase with the driving field. This is followed by collapse to the ground state, and subsequent detection of a fluctuation at time t' arising from the coherent dipole moment that is out of phase with the driving field. The second term interchanges the out of phase and in phase parts.

For large generalized Rabi frequencies, where $\beta' \tau_o \gg 1$, when the time average over t is performed in the correlation function, the second term in Eq. (8) is dominant, since it contains $[\sin(\theta' - \theta)]/4 = [\sin(\beta' \tau)]/4$ which is t independent. All other terms are down by a factor $(1/\beta' \tau_o)$. Hence, a particular time-ordered process is favored in this case. Evaluation of the power spectrum for this term shows that it is an odd function of $\omega - \beta'$ that causes the small squeezing of Fig. 8.

Using elementary trigonometric identities, Eq. (8) can be rewritten as

$$\frac{\beta_d^2 \Delta}{2\beta'^3} \left[\frac{\sin\theta}{2} \frac{1 - \cos\theta'}{2} - \frac{(1 - \cos\theta)}{2} \frac{\sin\theta'}{2} \right] \sin 2\phi. \tag{9}$$

A remarkable feature of Eq. (9) is the appearance of the *minus* sign between the two terms. Hence, the cross correlation appears odd in the interchange of t' and t. Note that Eq. (9) is valid for $t' = t + \tau \geq t$ only. For $\tau \leq 0$, the order is reversed, so that the correlation function actually is an even function of τ as it must be.

The minus sign in Eq. (9) can be shown to arise from the commutator of two positive frequency source field operators evaluated at times t and t', as discussed in Ref. [23]. This commutator enforces time ordering. The structure of Eq. (9) is identical to the quantum noise term described in Sec. V ($F_N \sin 2\phi$) that causes the difference in the $\pm 45°$ noise power spectra.

Equation (9) differs from the corresponding classical cross correlation between absorption and dispersion of atoms that cross the driving field. For the classical cross correlation, the minus sign is replaced by a *plus* sign: time ordering does not arise, as the radiator is not affected by the radiation process. The contributions of the classical cross correlation to the noise spectra are found to be negligible, as shown by the similarity of the spectra in Fig. 2. By contrast, the contribution to the quantum noise spectrum, for which the minus sign appears, is large. It can be shown that the ratio of the classically calculated and quantum mechanically calculated cross correlations is of order $1/\beta' \tau_o$, which is $\ll 1$ in our experiments.

The quantum noise spectrum includes also effects of phase-dependent spontaneous emission from the excited state, i.e., not arising from the coherent dipole. The presence of the driving field modulates the spontaneous dipole moment. The resulting power fluctuations depend on the relative phase between the LO and the driving field, leading to phase-dependent structure in the spontaneous noise spectrum. This structure is found to be identical for the $\pm 45°$ noise spectra. A more detailed description of the point of view presented briefly here will be given in a future publication.

III. EXPERIMENT

The present experiments, Fig. 3, measure phase-dependent resonance fluorescence spectra using a unique homodyne detection system. In this method, excess noise is suppressed by subtracting signals from two identical atomic samples, each prepared as described below. To implement this scheme, we employ a 1-cm-wide supersonic Yb beam which crosses two identical continuous laser field regions for which the power transmitted through the polarizer GP2 is monitored using two diode detectors. The 556-nm $^1S_0 \rightarrow {}^3P_1$ transition of ^{174}Yb forms a two-level system comprising the $J = 0$ state and the $J = 1$, $M = 1$ state with a radiative lifetime of 875 ns. Doppler shifts of the diverging supersonic beam are suppressed by applying a magnetic field gradient along the laser propagation direction **y** [46]. This magnetic compensation is possible for a supersonic beam, since, with a narrow spread in the atomic speed, there is approximately a linear relation between the Doppler shift and the position along **y** at which an atom intersects the driving laser beam. Magnetic compensation of the Doppler shifts is accomplished in the present experiments by using tilted pole pieces for which the gap varies in the **y** direction, Fig. 4. The gradient is adjusted to cancel the Doppler shifts by varying the total current in the magnet coils. The uniform component of the magnetic field along the **z** axis is used to split the $J = 1$ magnetic sublevels. Magnetic compensation greatly en-

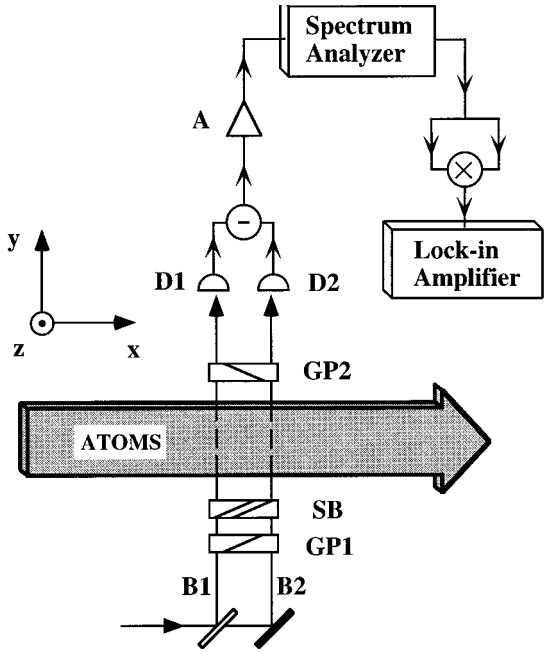

FIG. 3. Measurement of phase-dependent resonance fluorescence spectra by subtraction of transmitted power signals from two identically prepared atomic samples.

hances the intensity of the radiation field and simplifies data analysis, by permitting near-resonant excitation of the entire atomic volume with a driving field of well-defined detuning [47].

The laser frequency is offset locked to the atomic resonance with variable detuning to measure phase-dependent fluorescence spectra for on- or off-resonance excitation. This is accomplished by frequency shifting two beams derived from the same laser: the first (stronger) beam is shifted by 110 MHz using a fixed frequency acousto-optic (AO) modulator, the output of which provides LO and driving fields for the atoms; the second (weaker) beam is shifted using a tunable frequency AO modulator, the output of which is focused into a single mode optical fiber. The output direction of the beam from the fiber does not vary as the AO modulator is tuned. This beam passes through the atomic beam at a position where it does not affect the atoms used in the noise measurements. A discriminator signal for the servo system is obtained by synchronously detecting the absorption of this weak beam as the frequency of the tunable AO modulator is dithered.

A. Identical local oscillator fields

Two identical LO beams are created in the experiments, one for each interaction region. Each LO field has the same fixed, controllable phase with respect to the field that drives the atoms in its respective region. This is accomplished as follows. In each interaction region, atoms cross a strong continuous laser field that is polarized in the **x**-**z** plane by a glan prism GP1 oriented at an angle θ with respect to the **z** axis, Fig. 4. Only the **x** component $\mathcal{E}_x$ interacts with the atoms by exciting the $\Delta M=1$ transition. The $\mathcal{E}_z$ component is far off resonance with the $\Delta M=0$ transition, due to the strong applied uniform Zeeman field along the **z** direction, which

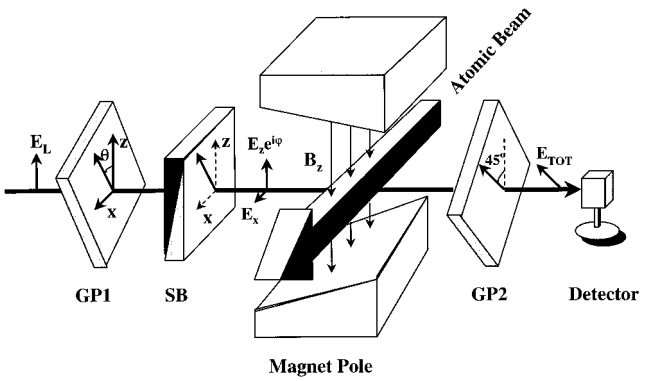

FIG. 4. Experimental scheme showing one of the preparation beams and the method for generating a local oscillator field with a stable phase.

splits the $J=1$, $M=0,\pm 1$ magnetic substates by approximately 1 GHz. For this reason, $\mathcal{E}_x$ is denoted as the *driving* field. The relative phase, $\varphi=\varphi_z-\varphi_x$, between the **z** and **x** components is determined by a Babinet-Soleil (SB) compensator. The polarizer GP2 defines a local oscillator field $\mathcal{E}_{\mathrm{LO}}$: this is the laser field transmitted through GP2. The axis of GP2 is oriented at 45° to the **z** axis, so that the **x**-polarized radiation field of the atoms is mixed with $\mathcal{E}_{\mathrm{LO}}$ to produce the total field at the detector. For this case, the LO field transmitted through GP2 in the absence of atoms is given by $\mathcal{E}_{\mathrm{LO}}=|\mathcal{E}_{\mathrm{LO}}|e^{i\phi}=\mathcal{E}_x/\sqrt{2}+\mathcal{E}_z e^{i\varphi}/\sqrt{2}$. The corresponding power is

$$P_{\mathrm{LO}}=\tfrac{1}{2}\left[P_x+P_z+2\sqrt{P_x P_z}\cos(\varphi_z-\varphi_x)\right]. \tag{10}$$

The relative phase between the LO field and the driving field, $\phi\equiv\phi_{\mathrm{LO}}-\varphi_x$, is determined from

$$\tan\phi=\frac{\sin(\varphi_z-\varphi_x)}{\cos(\varphi_z-\varphi_x)+\sqrt{P_x/P_z}}. \tag{11}$$

Hence, varying the phase of the SB compensator adjusts the relative phase ϕ between the driving field $\mathcal{E}_x$ and the net local oscillator field $\mathcal{E}_{\mathrm{LO}}$; this allows measurement of phase-dependent fluorescence spectra for well-defined quadrature components of the radiation field of the atoms.

We define the in phase and out of phase quadrature signals as those for $\phi=0°$ and $\phi=90°$, respectively, i.e., the local oscillator field is in phase or 90° out of phase with the driving field. Since the mean atomic radiation field is π out of phase with respect to the driving field (for atoms initially in the ground state), the relative phase between the LO field and *mean* atomic radiation field is well defined. Similarly, the LO phase is well defined relative to the mean atomic dipole moment, which is 90° out of phase with the mean atomic radiation field.

B. Subtraction of signals from identically prepared samples

One important feature of the experiments is the subtraction of signals from the two identical interaction regions to suppress excess noise, so that quantum noise in the quadrature signals can be measured. Each of these regions is placed so that different atoms are excited. Using this method, the

technical noise in the local oscillator subtracts. Since the total signals from the two regions are subtracted, this method also subtracts the excess noise in the nonvanishing quadrature signals [48], in contrast to homodyne detection with a beam splitter [49], where the nonvanishing quadrature signals add. This feature is important in the present experiments because the quadrature signals are large enough that the excess noise would dominate the quantum noise signals of interest. In contrast to the technical noise, which subtracts, the quantum noise from the two regions adds. This is due to the fact that the quantum fluctuations in the two radiating regions are independent, as the optical fields are generated with a beamsplitter and interact with independent atoms. A detailed discussion of this method is given in Appendix A.

Subtraction of signals from the interaction regions is implemented using diode detectors (EG&G FFD-040B) to monitor the signal fields transmitted through the projection polarizer. The detector outputs are subtracted and converted to a voltage by a low-noise transimpedance amplifier (Signetics NE5211, $R=14\mathrm{k}\Omega$). The detection system has a flat response to $\simeq 80$ MHz, well beyond the 20-MHz spectral range measured in the experiments. Noise voltage signals from the transimpedance amplifier are measured with a spectrum analyzer (HP 8553B).

C. Noise power spectra

Another important feature of the experiments is direct measurement of the mean-square optical noise voltage, i.e., the noise power spectrum, on a *linear* scale with high sensitivity. With this system, the atom contributions to the noise spectra are readily isolated from the shot-noise and electronic noise contributions. This technique is implemented using a method which is well known in light beating spectroscopy [50]: the voltage output of the analog spectrum analyzer is squared using a low-noise multiplier (Analog Devices AD-534K). The output of the multiplier then is fed to a lock-in amplifier (SR 850-DSP) which subtracts the mean square noise signals obtained with the laser fields on and off. In this way, the mean square electronic noise is subtracted in real time, and the lock-in output is proportional to the mean-square optical noise voltage [51].

As a calibration of the detection system, the mean-square shot-noise voltage is measured. In this case, the lock-in output scales linearly with the total power incident on the balanced detectors from 6 mW down to 2 μW. The measured slope agrees with predictions based on shot noise, the system gain factors and the detector efficiency to better than 10% [52].

Phase-dependent resonance fluorescence spectra are isolated by subtracting the shot-noise contribution. This is determined by measuring the on-resonance transmitted power P for a particular quadrature phase ϕ, just after a quadrature power spectrum is recorded. Then, with the laser far off resonance, the power is reset to P and the shot-noise spectrum is measured; this determines the shot-noise contribution to the measured power spectrum.

D. Experimental parameters

The detection system efficiency (including focusing lenses) is $\eta_o=0.51$, as determined from the measured photocurrent conversion factor of $\eta_o e/(\hbar\omega)=0.23$ A/W. The spectrum analyzer bandwidth used in these experiments is $\Delta\nu=100$ kHz. The $1/e$ field radii of the interaction regions are found to be $a=100$ μm along the atomic beam, and $b=0.76$ mm in the vertical direction. The supersonic speed is found to be $v=6\times10^4$ cm/s, as measured by time-of-flight methods. In the theory, the laser fields are assumed to have a square beam profile along the atomic beam axis. This simplifies calculation of the phase-dependent spectra, as described in Sec. V. Since the laser beams actually have a Gaussian profile, we take the effective transit time for an atom to cross a beam with a square profile to be $\tau_o=a\sqrt{\pi}/v=0.17\sqrt{\pi}$ μs.

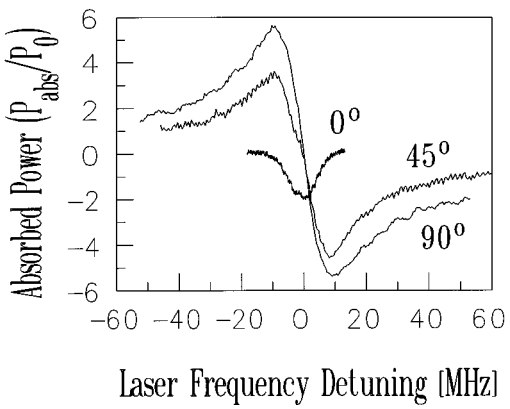

FIG. 5. Phase-dependent absorption as a function of laser frequency for the power transmitted through GP2 of Fig. 4. In the experiments, $P_x=1$ mW, $P_z=3$ mW, and $\phi=0°$, 45°, and 90°. The absorbed power is given in units of $P_o\equiv\dot{N}\hbar\Omega\sqrt{P_{\mathrm{LO}}/(2P_x)}$.

E. Phase-dependent absorption spectra

Phase-dependent absorption spectra as a function of the laser frequency have been measured for quadratures in phase ($\phi=0°$), out of phase ($\phi=90°$), and at $\phi=45°$ with respect to the driving field. These quadrature phase settings are determined by the Babinet compensator shown in Fig. 4. For each phase setting, the power absorbed from the beam transmitted through GP2 is measured as a function of laser frequency. These phase-dependent absorption spectra are shown in Fig. 5. The in-phase ($\phi=0°$) absorption spectrum is a symmetric, bell-shaped curve, centered at the atomic resonance frequency. By contrast, the out-of-phase ($\phi=90°$) absorption spectrum is an antisymmetric function of the laser frequency. The absorption vanishes at zero detuning. In this case, the mean atomic radiation field is 90° out of phase with the LO field, so that the transmitted power is unaffected until the laser is detuned from resonance, which changes the phase. The 45° absorption spectrum contains both symmetric and antisymmetric functions of the laser detuning.

IV. PHASE-DEPENDENT RESONANCE FLUORESCENCE SPECTRA

For each quadrature signal at a fixed driving field detuning, there is a phase-dependent resonance fluorescence spectrum measured as a function of spectrum analyzer frequency. This is the power spectrum of the fluctuations in the chosen quadrature. These power spectra are measured for both on-

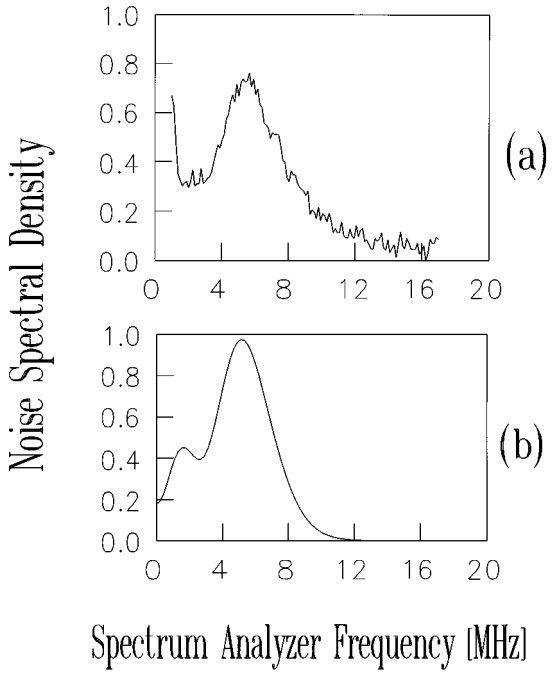

FIG. 6. Phase-dependent fluorescence spectra for coherently driven two-level atoms. (a) Measured in-phase ($\phi=0°$) noise spectrum for on-resonance excitation and effective pulse area $\theta_M=4\pi$. Here $\dot{N}\hbar\Omega=0.12$ mW is determined from the power absorbed from P_x on resonance; $P_x=1$ mW and $P_z=0$. The noise spectral density (V^2/Hz) was divided by the measured shot noise spectral density for 1 mW of total power; a noise spectral density of 0 corresponds to the shot noise level of the total transmitted power, which has been subtracted. (b) Calculated noise spectra using the same units as (a) and no free parameters. Both the data and the theory were divided by $P_{\rm LO}/(2P_x)$.

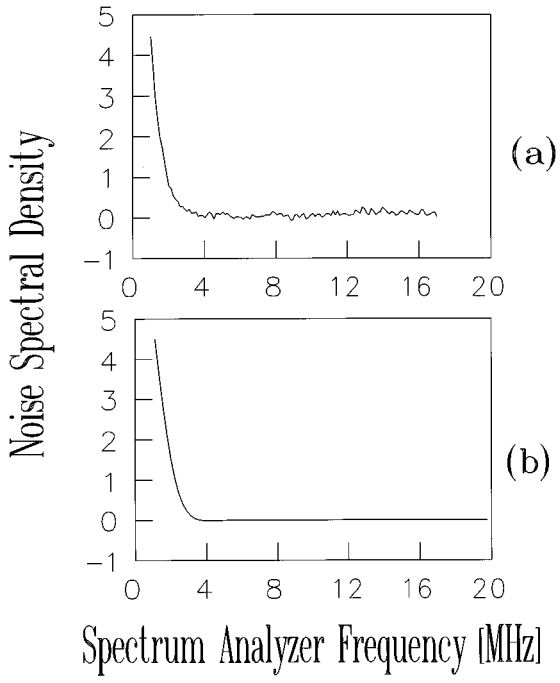

FIG. 7. Phase-dependent fluorescence spectra for coherently driven two-level atoms. (a) Measured out-of-phase ($\phi=90°$) noise spectrum for on-resonance excitation and effective pulse area $\theta_M=4\pi$. Here $\dot{N}\hbar\Omega=0.25$ mW is determined from the power absorbed from P_x on resonance; $P_x=1$ mW, $P_z=3$ mW, and $P_{\rm LO}=1$ mW. The noise spectral density (V^2/Hz) was divided by the measured shot noise spectral density for 1 mW of total power; a noise spectral density of 0 corresponds to the shot noise level of the total transmitted power, which has been subtracted. (b) Calculated noise spectra using the same units as (a) and no free parameters. Both the data and the theory were divided by $P_{\rm LO}/(2P_x)$.

and off-resonant driving fields. Phase-dependent fluorescence spectra for on-resonance excitation are shown in Fig. 6 for radiation in phase with the driving field ($\phi=0°$), and in Fig. 7 for radiation out of phase with the driving field ($\phi=90°$). The driving field is tuned to resonance with a maximum pulse area (for atoms crossing the center of the interaction region) of $\theta_M=4\pi$ at a driving field power of 1 mW.

The zero level of power spectral density corresponds to the shot noise level of the total transmitted power which has been subtracted. The baseline is not adjusted after subtraction of the shot noise. The remaining atom-noise spectral density has been divided by the dimensionless ratio $P_{\rm LO}(\phi)/(2P_x)$, which is phase dependent (see Sec. V). One unit of spectral density is the shot-noise spectral density (V^2/Hz) for 1 mW of total power. Since the LO beam powers typically are of order 1 mW, the shot-noise spectral density of a 1-mW beam is a convenient unit. Note that an accurate measurement of the power spectrum requires noise sensitivity well below this level.

Figure 8 shows the corresponding noise spectra for 180 $\pm 45°$ quadratures. Here, the driving field is -6.6 MHz off-resonance with a maximum pulse area (on resonance) of $\theta_M=5.6\pi$ at 2 mW of driving field power.

A. On-resonance noise spectra

For the in-phase measurements, the driving beam power is $P_x=1.0$ mW (one region) to obtain a maximum pulse area $\theta_M=4\pi$. To measure the $\phi=0°$ quadrature noise spectrum shown in Fig 6(a), the power in the **z**-polarized field for each interaction region is $P_z=0$, and the polarizer GP2 is removed. Similar noise spectra are obtained for $P_z\neq 0$ and $\phi=0°$ with GP2 installed. This is as it should be, since the in-phase data is equivalent to the absorption noise of a strong beam. For the out-of-phase data, again $P_x=1$ mW, but the power in the **z**-polarized beam is taken to be $P_z=3.0$ mW, and the Soleil-Babinet compensator is adjusted to give $\varphi_z-\varphi_x=125°$ so that the denominator of Eq. (11) vanishes and $\phi=\pi/2$. Equation (10) yields the LO power $P_{\rm LO}=1$ mW as measured in the experiments. For comparison with the theoretical power spectra (see Sec. V), we require $\dot{N}$, the number of atom/s crossing one interaction region. From the measured absorption of the transmitted driving beam on resonance, $\dot{N}\hbar\Omega$ is determined to be $\simeq 0.12$ mW for the $\phi=0°$ data, and 0.25 mW for the $\phi=90°$ data.

The measured on-resonance in-phase noise spectrum, [Fig. 6(a)] exhibits a number of interesting features. The in-phase spectrum appears as a broad peak centered near the Rabi frequency of the driving field, and exhibits a local minimum near 2.5 MHz. By contrast, the out-of-phase spectrum,

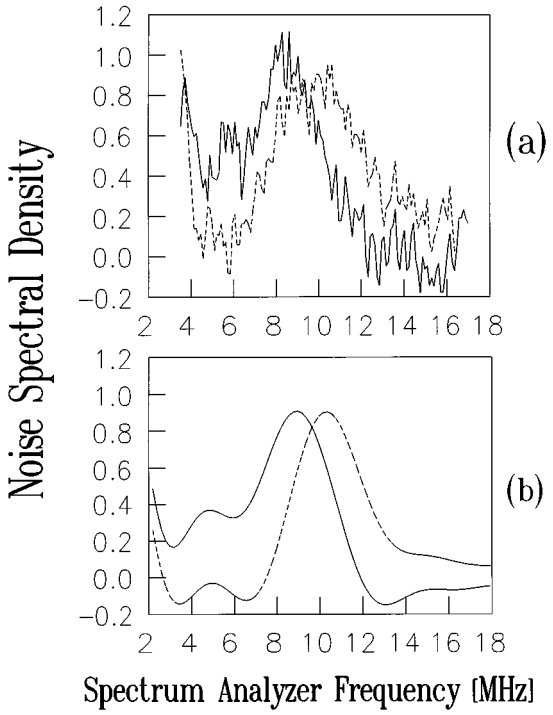

FIG. 8. Phase-dependent fluorescence spectra for coherently driven two-level atoms. (a) Measured noise spectra for $\phi = 135°$ (solid line) and 225° (dashed line) at a laser detuning of -6.6 ± 1 MHz and an effective pulse area $\theta_M = 5.6\pi$. $P_x = 2$ mW, $P_z = 9$ mW, and $P_{\rm LO} = 1.67$ mW. $\dot{N}\hbar\Omega = 0.13$ mW is determined by the power absorbed from the P_x beam when it is on resonance. The noise spectral density (V^2/Hz) was divided by the shot noise spectral density for 1 mW of total power. (b) Calculated noise spectra using the same parameters as (a) except $\Delta = -5.8$ MHz. Both the data and the theory were divided by $P_{\rm LO}/(2P_x)$.

[Fig. 7(a)] is centered at zero frequency, and is small near the Rabi sidebands. Spectra of this general structure have been predicted previously for short-lived atoms driven with a Rabi frequency greater than the spontaneous decay rate [35,53]. The out-of-phase noise approaches zero at high frequency, and it exceeds the in-phase noise at low frequency. For equal values of $\dot{N}$, the in-phase and out-of-phase spectra cross near 2 MHz. At this frequency, the phase-dependent noise vanishes, leaving only the phase-independent contribution. It is interesting to note that the average of the in-phase and out-of-phase spectra yields the phase-independent part of the noise spectrum (see Sec. V). This average noise spectrum is equivalent to a fluorescence spectrum, with spectral resolution limited by the transit time across the local oscillator beam. The average of the measured noise spectra exhibits peaks centered at zero frequency and near the Rabi sidebands, similar to a Mollow spectrum [3].

B. Off-resonance noise spectra

For these experiments, the driving beam power is $P_x = 2$ mW, and $\theta_M = 5.6\pi$. The power in the **z**-polarized beam is $P_z = 9$ mW. From the measured absorption of the 2-mW driving beam, we find $\dot{N}\hbar\Omega = 0.13$ mW.

By using a large P_z, the LO field is rendered relatively insensitive to phase shifts due to the medium. In order to keep the LO power at a modest level, the Babinet compensator is adjusted to give $\varphi_z - \varphi_x = 154°$ or 206°, so that the quadrature phases used in the experiments are $\phi = 135°$ and 225°, respectively, according to Eq. (11). Using Eq. (10), the corresponding LO power $P_{\rm LO} = 1.67$ mW in both cases, as measured in the experiments. In the actual experiments, the Babinet compensator is adjusted slightly to yield identical LO powers for the two quadratures. This compensates for a small phase shift induced in the off-resonant driving beam by the medium.

With the laser offset-locked off-resonance by approximately -6.6 ± 1 MHz, phase-dependent resonance fluorescence spectra are obtained for $\phi = 180 \pm 45°$ quadratures. As shown in Fig. 8(a), these spectra are quite different. The two spectra cross near 10 MHz. The $+135°$ plot has a high level at low frequency, rises to a maximum near 8 MHz, and descends to a minimum near 12 MHz, where it probably dips below the shot-noise level, indicating a small amount of squeezing. By contrast, the 225° noise spectrum starts out low at low frequency, where it may be dipping below the shot-noise level. It crosses the 135° data, rises to a maximum, and then descends to a level well above the shot-noise level at the highest frequency shown.

V. THEORY

In our experiments, phase-dependent absorption is observed and phase-dependent noise is measured for various phase quadratures of the radiation field emitted by many atoms in the forward direction. This system is similar to that analyzed theoretically by Heidmann and Reynaud [37]. The experimental noise spectra obtained for resonant excitation with $\phi = 0°$ and 90° are in good qualitative agreement with predictions by Collett, Walls, and Zoller [35], as described above. In this section, we present a quantum treatment of the expected noise spectra for long-lived atoms, without invoking the quantum regression theorem. The predicted noise spectra are in excellent quantitative agreement with the measured spectra for both on- and off-resonant excitation.

We review the basic physics of two-level atom noise spectra for a thin sample of coherently driven long-lived two-level atoms in an atomic beam. We begin with a heuristic estimate of the magnitude of the phase-dependent absorption and atom noise signals. Then, the results of a more complete quantum mechanical treatment of the noise spectra (Appendix B) are described.

A. Atom-noise estimate

The form and magnitude of the phase-dependent absorption and noise for resonant excitation can be estimated using heuristic arguments. Denoting the radiation field of a single atom by $\vec{\mathcal{E}}_s$, the corresponding change in the power transmitted through GP2 (Fig. 4) is $\Delta P^{(1)} \simeq (c/8\pi) 2 \vec{\mathcal{E}}_{\rm LO} \cdot \vec{\mathcal{E}}_s A$, where A is the cross-sectional area of the local oscillator beam. With a dipole μ in the volume AL, the radiation field in the paraxial approximation (i.e., in the near forward direction where the local oscillator field is nonzero) is $\vec{\mathcal{E}}_s \simeq 2\pi i (\Omega/c) L (\mu/AL) \hat{x}$, where Ω is the frequency of the optical field. This leads to a net power change per atom of $\Delta P^{(1)} \simeq (\hbar\Omega/2)(\mu \hat{x} \cdot \vec{\mathcal{E}}_{\rm LO}/\hbar)$. This can be rewritten in terms

of the pulse area, $\theta_M \simeq \mu \mathcal{E}_x \tau_o/\hbar$, where τ_o is the transit time of the atom to cross the interaction region; $\Delta P^{(1)} \simeq (\hbar\Omega/2)(\theta_M/\tau_o)\hat{x}\cdot\vec{\mathcal{E}}_{\rm LO}/\mathcal{E}_x$. With the local oscillator polarization at 45° to the **x** axis, $\hat{x}\cdot\vec{\mathcal{E}}_{\rm LO}/\mathcal{E}_x = \sqrt{P_{\rm LO}/(2P_x)}$, and the absorbed power per atom is of order

$$\Delta P^{(1)} = \frac{\hbar\Omega}{2}\frac{\theta_M}{\tau_o}\sqrt{\frac{P_{\rm LO}}{2P_x}}, \tag{12}$$

where P_x and $P_{\rm LO}$ are the driving field and LO powers, respectively.

For N interacting atoms in the volume, we can define $\dot{N} = N/\tau_o$ as the rate at which atoms traverse one interaction region. Then the power absorbed from the beam transmitted through GP2 is of order $N\Delta P^{(1)}$, or

$$P_{\rm ABS} \simeq -\dot{N}\hbar\Omega\sqrt{\frac{P_{\rm LO}}{2P_x}}, \tag{13}$$

assuming strong excitation where $\theta_M \simeq 1$. The natural scale of absorbed power for an atom with a long radiative lifetime corresponds to one photon being absorbed for each atom that traverses the interaction region.

The magnitude of the phase-dependent optical noise per unit bandwidth, $S(\nu)$, which is studied in the experiments, also can be understood using heuristic arguments. For each atom that crosses the interaction region, the atomic dipole moment causes a power change of order $P^{(1)}$ in Eq. (12). Since the atoms arrive independently, the mean-square power fluctuation is of order $N[\Delta P^{(1)}]^2$, and is distributed over a bandwidth $\simeq 1/\tau_o$. It is not difficult to show that $N[\Delta P^{(1)}]^2$ is of order $NP_{\rm LO}P_{\rm Spont}$, where $P_{\rm Spont}$ is the spontaneous power radiated by one atom into the diffraction angle of the LO. Using Eq. (12), the mean-square power noise in a bandwidth $\Delta\nu$ is of order

$$S(\nu)\Delta\nu \simeq N[\Delta P^{(1)}]^2\tau_o\Delta\nu \simeq \Delta\nu\dot{N}\left(\frac{\hbar\Omega}{2}\right)^2\theta_M^2\frac{P_{\rm LO}}{2P_x}. \tag{14}$$

From Eqs. (14) and (13), we see the natural scale of the atomic contribution to the optical noise in the transmitted beam: it is the order of the shot noise corresponding to the absorbed power, i.e., of order $P_{\rm ABS}\hbar\Omega\Delta\nu$.

B. Phase-dependent resonance fluorescence spectra

Measurement of phase-dependent resonance fluorescence spectra permits a study of the atomic contributions to the noise in the radiation field of the driven samples. For a thin sample and long-lived atoms, these phase-dependent noise spectra can be understood from the decay-free operator optical Bloch equations for the independent two-level atoms, as described in detail in Appendix B. Appendix B describes the calculation of the dipole autocorrelation function for the long-lived atoms, using the Bloch vector operator evolution equations. The noise power spectrum is calculated from the normal and time-ordered power autocorrelation function, and has a magnitude in agreement with the heuristic estimate of Eq. (14). This power spectrum can be written in terms of distinct noise sources according to Eq. (B43) in the form

$$S(\nu,\phi)\Delta\nu = \eta_S P + \eta_S\dot{N}\hbar\Omega\left(\frac{P_{\rm LO}}{2P_x}\right)\frac{\eta_o}{4}\theta_M^2\{[F_D(\nu)+F_{\rm SP}(\nu)] + [F_D(\nu)+F_B(\nu)]\cos 2\phi + F_N(\nu)\sin 2\phi\}, \tag{15}$$

where $\phi \equiv \phi_{\rm LO} - \varphi_x$ and we have taken $P_p = P_x$ and $\phi_p \equiv \varphi_x$ in Eq. (B43). The first term in Eq. (15) is the mean-square shot noise due to the total (both regions) transmitted power P. The terms $\propto \dot{N}\hbar\Omega$ are the atom-noise contributions, as described below. The rate $\dot{N}$ at which atoms cross a single interaction region is determined by measuring the total power absorbed from a pure **x**-polarized beam as described below. In Eq. (15), ν ($\Delta\nu$) is the spectrum analyzer frequency (bandwidth) in Hz. $\eta_S \equiv 2\hbar\Omega\eta_o\Delta\nu$, with η_o the detection system efficiency. $P_{\rm LO}$ (P_x) is the total transmitted (driving) field power with the laser fields off resonance. The maximum Bloch angle is $\theta_M = \beta_x\tau_o$. The driving field Rabi frequency β_x, detuning Δ, and the transit time τ_o for atoms to cross an interaction region determine the frequency scales of the dimensionless spectral functions, $F_D(\nu)$, etc.

As shown in Appendix B, we find

$$\begin{aligned} F_D(\nu) &= F[\sin\theta,\sin\theta;\nu], \\ F_{\rm SP}(\nu) &= F[1-\cos\theta,1-\cos\theta;\nu], \\ F_B(\nu) &= F[\cos\theta+1,\cos\theta-1;\nu], \\ F_N(\nu) &= \Delta\tau_o\left\{F\left[1-\cos\theta,\frac{\sin\theta}{\theta_M'}\right]-F\left[\frac{\sin\theta}{\theta_M'},1-\cos\theta\right]\right\}. \end{aligned} \tag{16}$$

Here $F[f,g,\nu]$ takes the form

$$F[f(\theta),g(\theta);\nu] = 2\ {\rm Re}\int_0^1 d\tilde{\tau}\ e^{-i2\pi\nu\tau_o\tilde{\tau}}C[f(\theta),g(\theta);\tilde{\tau}], \tag{17}$$

where $C[f,g,\tilde{\tau}]$ is a normal and time-ordered correlation function given by

$$\begin{aligned} &C[f(\theta),g(\theta);\tilde{\tau}] \\ &\quad = \int_{-\infty}^{\infty}\frac{d\eta}{\sqrt{\pi}}e^{-2\eta^2}\int_{-(1/2)}^{(1/2)-\tilde{\tau}}d\xi\ \frac{\theta_M^2 e^{-2\eta^2}}{\theta_M'^2(\eta)} \\ &\qquad \times f[\theta(\xi+\tilde{\tau},\eta)]g[\theta(\xi,\eta)]. \end{aligned} \tag{18}$$

In Eq. (18), the integral over the dimensionless variable $\eta = z/b$ averages the correlation function in the vertical direction, where the field $1/e$ radius is b. The integral over the dimensionless variable $\xi = x/a$ determines the correlation along the atomic beam axis **x**. a is the full width of the field, which is assumed to have a rectangular profile along the atomic beam. This simplifies the calculations for off-resonant excitation. The position-dependent effective Bloch angle is given by

$$\theta(\xi,\eta) = \theta_M'(\eta)(\tfrac{1}{2}+\xi), \tag{19}$$

with the effective maximum pulse area

$$\theta'_M(\eta) \equiv \sqrt{\theta_M^2 \exp(-2\eta^2) + (\Delta\tau_o)^2}. \quad (20)$$

Note that the left argument of $C[f,g;\tilde{\tau}]$, f, is evaluated at a later time, $\xi+\tilde{\tau}$, than the right argument g, which is evaluated at ξ. Hence F_D and $F_{\rm SP}$ are symmetric under the interchange of time ordering, F_B has both even and odd contributions, and F_N is antisymmetric under the interchange of the time ordering [23].

Corresponding to the phase-dependent noise spectra, the phase-dependent power absorbed as a function of driving field frequency is given by Eq. (B49). The rate at which atoms cross one region, $\dot{N}$, is determined by measuring the total power absorbed from a resonant **x**-polarized driving field, with the polarizer GP2 of Fig. 4 removed. In this case, the factor $P_{\rm LO}/(2P_x)\rightarrow 1$ in Eq. (B49), $F_c\rightarrow F_o$ and $F_s\rightarrow 0$. $\dot{N}$ for one region is determined from the total power absorbed from both regions on resonance using

$$P^x_{\rm ABS} = -\dot{N}\hbar\Omega F_o(\theta_M), \quad (21)$$

where

$$F_o(\theta_M) = \int_{-\infty}^{\infty} \frac{d\eta}{\sqrt{\pi}} e^{-2\eta^2}[1-\cos(\theta_M e^{-\eta^2})]. \quad (22)$$

Note that $F_o(\theta_M)/2$ is just the mean excitation probability for an atom which traverses one interaction region.

Atom noise contributions

The first four atomic contributions that appear in Eq. (15) have been discussed previously [22]. The first two terms $F_D+F_{\rm SP}$ are phase independent, and are similar to an ordinary resonance fluorescence spectrum [3,54]. This spectrum arises from a sum of elastic and inelastic scattering. As shown previously for long-lived excited states, the sum of the probabilities for the atom to arrive in the ground state, emit one photon and exit in the ground or excited states yields the fluorescence spectrum [55]. For on-resonance excitation, $F_D(1+\cos 2\phi)$ describes noise arising from the mean dipole moment of single atoms that traverse the interaction region, while $F_{\rm SP}$ describes the phase independent part of the fluctuating atomic dipole moment [14]. The $F_B\cos 2\phi$ term can be considered to arise from phase-dependent fluctuations in the in and out-of-phase quadrature components of the atomic Bloch vector [22].

The novel spectral features observed in Fig. 8 for off-resonance excitation with $\phi = 180 \pm 45°$ are described by the last term of Eq. (15), $F_N(\nu)\sin 2\phi$. This term causes the striking asymmetry between these power spectra. It vanishes at zero detuning and for the in-phase ($\phi = 0°$) and out-of-phase quadratures ($\phi = 90°$). Hence it was not measurable in our first experiment [22]. The structure of F_N shows that it arises from atomic operator products that are odd under the exchange of time ordering as described above. Hence it is easy to see that this contribution would vanish if symmetric time ordering were chosen arbitrarily [23]. The effects of $F_N(\nu)$ are isolated in the experiments, since $\cos 2\phi = 0$ for $\phi = 135°$ and $225°$, while $\sin 2\phi = \mp 1$.

VI. THEORETICAL PHASE-DEPENDENT FLUORESCENCE SPECTRA

Using Eq. (15), phase-dependent fluorescence spectra can be calculated in absolute units, using the experimentally measured parameters.

A. On-resonance

The measured on-resonance noise spectra can be compared to those calculated from Eq. (15) for $\phi = 0°$ and $90°$. Figures 6(b) and 7(b) show the calculated phase-dependent noise spectral density $[S(\nu) - \eta_S P]/\eta_S$, in units of the shot-noise spectral density, for 1 mW. The spectra were calculated from Eq. (15) using the experimentally determined parameters. However, the spectral functions, F_D, etc., were determined using the Gaussian beam results of Ref. [22]. This was done to eliminate minor oscillations which arise from the square beam profile assumed in the present work. Except for these minor oscillations, the square beam results are in good agreement in both form and magnitude with the Gaussian beam results for the on-resonance case. Both the predictions and the data have been divided by the factor $P_{\rm LO}/2P_x$, the ratio of the phase-dependent local oscillator power to the driving field power.

The observed spectra have a shape and magnitude in excellent agreement with the predictions, using no free parameters. For the in-phase spectrum, the broad peak centered near the Rabi sidebands arises from three terms: $F_{\rm SP}$ and F_B add to contribute half of the amplitude, while the phase dependent and independent contributions from F_D provide the other half. Note that the mean dipole moment terms F_D do not have an ''elastic'' in-phase peak, centered near zero frequency, as is the case for short lived atoms [14]. For the long-lived atoms used in this experiment, the mean dipole moment is modulated at the Rabi frequency and the noise spectral function $F_D(\nu)$ is centered in the Rabi sidebands. For the out-of-phase spectrum, the mean dipole moment does not contribute, and $F_{\rm SP}$ and F_B are subtracted to produce the central peak.

As noted above, at a frequency of 2 MHz, the in-phase and out-of-phase noise components are of equal magnitude, and the phase-dependent noise contribution vanishes. In this case, the mean dipole noise increases the net noise level by exactly the same amount that the phase-dependent projection noise decreases it. It is interesting to note that in a system with a prepared Bloch vector where the Bloch angle θ is time independent, the net phase-dependent noise contribution to the spectrum vanishes for all ν.

The agreement between the data and theory in the present experiments is somewhat better than that of our previously published results [22]. Both the shape and magnitude of the data are in excellent agreement with the theoretical predictions. This is a consequence of improving the method of determining $\dot{N}$, which is now obtained directly from the absorption of a strong resonant beam, with GP2 removed. Further, the magnetic compensation of the Doppler shifts is optimized midway between the two interactions, which improves noise subtraction and reduces the absorption linewidth by reducing the Doppler broadening contribution.

B. Off-resonance

The off-resonance noise spectra can be compared to those predicted using Eq. (15) for $\phi = 180 \pm 45°$. The theoretical noise spectra are evaluated for $\Delta = -5.8$ MHz, which yields spectra centered near 10 MHz as in the experiments.

The agreement between the measured and predicted spectra [Fig. 8(b)] is excellent. Although the data are not quiet enough to conclusively verify the existence of the predicted squeezing, the data are of exactly the correct magnitude and they exhibit all of the correct qualitative features. A particularly interesting feature of this data is that it directly exhibits a manifestation of time ordering of the atomic operators as discussed above. If the atomic operators were arbitrarily ordered symmetrically, the term $F_N(\nu)$ in Eq. (15) would vanish, and the $180 \pm 45°$ quadrature noise spectra would be identical. Instead, they are quite different.

As described in Sec. II, the asymmetry of the $180 \pm 45°$ spectra cannot be interpreted in terms of the cross correlation between fluctuations in the *classical* dispersion and absorption from individual atoms which randomly pass through the interaction regions. When the classical contribution to the spectrum is calculated from the correlation function for the mean dipole moment of the atom, treated as a classical dipole, a cross correlation between absorptive and dispersive contributions does arise. It is $\propto \sin 2\phi$, but it is time symmetric in the atom source field operators, and fails to display the observed difference between the $180 \pm 45°$ spectra [23].

A physical interpretation for the asymmetry between the $180 \pm 45°$ spectra can be given for long-lived atoms. As described in Sec. II, a collapse to the ground state following detection of a photon is the key difference between the quantum and classical evolution of the coherent atomic dipole moment. This leads to time ordering and to the correct cross correlation between absorptive and dispersive power fluctuations.

VII. CONCLUSIONS

We have measured phase-dependent resonance fluorescence spectra for an elementary system: driven long-lived two-level atoms in an atomic beam. Phase-dependent resonance fluorescence spectra are very rich compared to those of ordinary resonance fluorescence spectra which are measured without phase sensitivity. By analyzing the quadrature power spectra of this simple radiating system, it has been possible to explore a number of phase-dependent atom noise sources in some detail. We have shown that striking manifestations of time ordering appear in the phase-dependent fluorescence spectra for off-resonant excitation.

For two-level atoms with a long radiative lifetime, the dipole autocorrelation function can be calculated without invoking the quantum regression theorem. The resulting theoretical spectra are in excellent agreement with the data, and have a relatively simple structure that is amenable to rigorous physical interpretation using the Bloch picture. This will be the subject of a future paper.

To our knowledge, a complete description of the *phase-dependent* fluorescence spectra in terms of simple scattering diagrams does not yet exist. The exploration of such a picture will provide further insights into the physical processes responsible for phase-dependent noise and time ordering in this elementary two-level quantum system.

The techniques employed in the measurements can be used to study noise in the radiation fields of atoms in a variety of configurations. These include atoms in dense Doppler-compensated beams [46,47] where, for example, it will be possible to explore phase-dependent noise spectra in cooperative emission and in three level systems exhibiting electromagnetically induced transparency.

ACKNOWLEDGMENTS

This work was supported in part by the National Science Foundation, the Rome Air Development Center, the U.S. Air Force Office of Sponsored Research, and the U.S. Army Research Office. We thank Professor D. Gauthier, Professor H. Carmichael, and Professor P. Berman for many stimulating conversations regarding this work.

APPENDIX A: SUBTRACTION OF IDENTICAL SIGNALS

In the experiments, technical noise in the transmitted power is suppressed by subtracting the signals from two independent samples of atoms, instead of using balanced homodyne detection with a beam splitter. These technical noise contributions arise in two ways. The first is just the direct fluctuation in the transmitted beam, which would contribute in the absence of atoms, i.e., the classical fluctuations in the effective LO. Additional technical noise arises from classical fluctuations in the interference between the LO field and the mean field emitted by the atoms, i.e., in the quadrature signals themselves. These multiplicative technical noise terms can arise from classical fluctuations in the driving field, which leads to classical noise in the radiation field of the atoms or from fluctuations in the net LO field, which interferes with the average radiation field of the atoms. While the noise which arises directly from the LO can be suppressed in ordinary balanced homodyne detection with a beam splitter, the interference terms add in this case, and hence the multiplicative noise terms add. For strongly radiating atomic samples, the failure of balanced homodyne detection with a beam splitter to suppress these multiplicative noise contributions leads to substantial technical noise in the measured noise spectra at low frequencies. By contrast, for atomic samples which are nominally identical, the method of subtracting signals from two independent regions suppresses the technical noise contributions in both the LO and in the phase-dependent quadrature signals of the atoms as well. This method is analyzed in this section for a thin sample.

Let $\hat{P}_i(t)$ be the Heisenberg operator for the total transmitted power for each sample $i = 1$ and 2. The operator corresponding to the difference in the transmitted powers is

$$\Delta \hat{P}(t) = \hat{P}_1(t) - \hat{P}_2(t). \tag{A1}$$

For ideal photodiodes, the one-sided $(\omega \geqslant 0)$ power spectrum of the difference current is proportional to that of the power difference operator,

$$S_{\Delta P}(\omega) = 2 \int_{-\infty}^{\infty} d\tau \frac{e^{i\omega\tau}}{2\pi} C_{\Delta P}(\tau) \tag{A2}$$

where $C_{\Delta P}(\tau)$ is the time and quantum averaged autocorrelation function of the power difference operator

$$C_{\Delta P}(\tau)=\langle C(t,t'=t+\tau)\rangle_T. \tag{A3}$$

Here T denotes an average over the time t, and $t'\geqslant t$ for $\tau \geqslant 0$. The quantum-averaged correlation function is given by

$$C(t,t')=\langle \Delta\hat{P}(t)\Delta\hat{P}(t')\rangle_Q, \tag{A4}$$

where Q denotes a quantum statistical average. We assume that the field modes are in a vacuum state except for a strong local oscillator mode.

The correlation function can be expanded in terms of the transmitted power operators for the two samples

$$C(t,t')=\langle(\hat{P}_1-\hat{P}_2)(\hat{P}'_1-\hat{P}'_2)\rangle_Q=\langle\hat{P}_1\hat{P}'_1\rangle_Q-\langle\hat{P}_1\hat{P}'_2\rangle_Q +\langle\hat{P}_2\hat{P}'_2\rangle_Q-\langle\hat{P}_2\hat{P}'_1\rangle_Q, \tag{A5}$$

where $\hat{P}=\hat{P}(t)$ and $\hat{P}'=\hat{P}(t')$.

The power operators are written in terms of the slowly varying field operators at the detectors, $\hat{\mathcal{E}}_i(t,\vec{x}_\perp)$, $i=1$ and 2, where the plane of the detector is denoted by $y=y_D=$ const, and $\vec{x}_\perp$ is a vector in the detector plane. Then, the cycle averaged power operator is taken as

$$\hat{P}_i(t)=\frac{c}{8\pi}\int d^2\vec{x}_\perp\hat{\mathcal{E}}^\dagger(t,\vec{x}_\perp)\hat{\mathcal{E}}(t,\vec{x}_\perp). \tag{A6}$$

In Eq. (A6), we assumed that the fields propagate nominally along **y**, and comprise a band of frequencies centered around the optical frequency Ω, so that

$$E_i(\vec{x},t)=\tfrac{1}{2}\hat{\mathcal{E}}_i(t,\vec{x}_\perp)e^{iqy-i\Omega t}+\text{H.c.} \tag{A7}$$

We assume that the total field operators at each detector are in source free regions, and therefore have the same commutators as free fields. In this case, the slowly varying field operators in a fixed plane (y) for samples $i=1$ and 2 are readily shown to obey approximately the commutation relations

$$[\hat{\mathcal{E}}_i(t,\vec{x}_\perp),\hat{\mathcal{E}}_j^\dagger(t',\vec{x}'_\perp)]=\frac{8\pi\hbar\Omega}{c}\delta(\vec{x}_\perp-\vec{x}'_\perp)\delta(t-t')\delta_{ij}. \tag{A8}$$

We assume in writing Eq. (A8) that the driving and local oscillator fields for samples 1 and 2 are derived using a beam splitter, and that the samples consist of different atoms, so that the total field operators for different samples commute.

The correlation functions appearing in Eq. (A5) can be rewritten using Eqs. (A6) and (A8). Incorporating the detection efficiency η_o in the usual way [48] yields

$$\langle\hat{P}_i\hat{P}'_j\rangle_Q=\delta_{ij}\eta_o\langle\hat{P}_i\rangle_Q\hbar\Omega\,\delta(t-t')+\eta_o^2\langle:\hat{P}_i\hat{P}'_j:\rangle_Q, \tag{A9}$$

where the first term is the shot noise of the total power for a single sample, and the double dots in the second term denote normal and time ordering. With Eq. (A9), the correlation function of Eq. (A5) can be written in the form

$$C(t,t')=\eta_o\langle\hat{P}_1(t)+\hat{P}_2(t)\rangle_Q\hbar\Omega\,\delta(t'-t) +\eta_o^2[C_{12}(t,t')+C_{21}(t,t')], \tag{A10}$$

where

$$C_{12}(t,t')=\langle:\hat{P}_1\hat{P}'_1:\rangle_Q-\langle:\hat{P}_1\hat{P}'_2:\rangle_Q, \tag{A11}$$

and $C_{21}(t,t')$ is identical in form to Eq. (A11), with $1\leftrightarrow 2$.

With Eq. (A10), the power spectrum, Eq. (A2), takes the form

$$S_{\Delta P}(\omega)=\eta_o\frac{\hbar\Omega}{\pi}P+\eta_o^2\frac{2}{\pi}\,\text{Re}\int_0^\infty d\tau\, e^{i\omega\tau}\langle C_{12}(t,t'=t+\tau) +C_{21}(t,t'=t+\tau)\rangle_T, \tag{A12}$$

where P is the total average transmitted power from the two samples (including the absorption). Note that the correlation function C_{12}, which describes the atom contribution to the power spectrum, is symmetric in τ, so that we take $\tau\geqslant 0$ in Eq. (A12) and in the following discussion.

The correlation functions C_{12} and C_{21} can be written in terms of the the total field, $\hat{\mathcal{E}}_i(t)$ at each detector, $i=1$ and 2; for example,

$$\langle:\hat{P}_1\hat{P}'_1:\rangle=\left(\frac{c}{8\pi}\right)^2\int d^2\vec{x}_\perp\int d^2\vec{x}'_\perp\langle\hat{\mathcal{E}}_1^\dagger\hat{\mathcal{E}}_1^{\dagger\prime}\hat{\mathcal{E}}'_1\hat{\mathcal{E}}_1\rangle_Q. \tag{A13}$$

Here we omit the spatial arguments for the field operators and $\hat{\mathcal{E}}_1\equiv\hat{\mathcal{E}}_1(t)$ and $\hat{\mathcal{E}}'_1\equiv\hat{\mathcal{E}}_1(t')$. For the normal-ordered correlation functions, the ordering of the total fields has been chosen as time ordered, with positive frequency field operators $\hat{\mathcal{E}}$ which are evaluated at later times placed to the left of those evaluated at earlier times. For the negative frequency fields, $\hat{\mathcal{E}}^\dagger$, the time ordering is reversed. This yields a manifestly Hermitian correlation function. Since the positive (or negative) frequency operators for the total fields commute, this ordering is arbitrary. However, the choice of time ordering simplifies the evaluation of the correlation functions, as is well known [37], and employed below.

The total field operators for the ith sample can be written in the form

$$\hat{\mathcal{E}}_i(t)=\mathcal{E}_{\text{LO};i}(t)+\hat{\mathcal{E}}_{V;i}(t)+\hat{\mathcal{E}}_{S;i}(t). \tag{A14}$$

The first term in Eq. (A14) is the local oscillator field, which is modelled as a strong classical field. It is the net laser field transmitted through the projection polarizer (Fig. 3) in the absence of the atoms. The second term is the corresponding vacuum field, which is responsible for the shot noise in the local oscillator power in the absence of atoms. Finally, the third term is the field from the atomic source.

The choice of normal and time ordering allows elimination of the explicit vacuum field operators from the expression for the correlation function. The vacuum field operators which appear in the outer total field operators of Eq. (A13) are immediately eliminated, since they act on vacuum states. This leaves only the classical local oscillator field and the source field in these outer factors.

Since the total fields have free-field commutators, the vacuum and source field terms generally do not commute. This is due to the interaction between the vacuum fluctuations and the source atoms. Vacuum fluctuations polarized along the driving field axis (**x**) can modify the dipole moment of the moving atoms, which then radiates a field in response to the fluctuations. As the dipole is affected only by vacuum fluctuations in the past, $\hat{\mathcal{E}}_{S;i}(t)$ contains vacuum field operators evaluated at times $\leqslant t$. Hence vacuum field operators, $\hat{\mathcal{E}}_{V;i}(t')$, evaluated at time $t' \geqslant t$ commute with $\hat{\mathcal{E}}_{S;i}(t)$. Since $t' = t + \tau \geqslant t$, for $\tau \geqslant 0$ as required according to Eq. (A12), we have $[\hat{\mathcal{E}}'_{V;i}, \hat{\mathcal{E}}_{S;i}] = 0$, as discussed previously [37]. Hence, the vacuum field operators which appear in the inner field operators of Eq. (A13) and which are evaluated later in time than the outer field operators commute with the later. Thus they can be commuted to the outside to act on the vacuum state, and are eliminated.

With the explicit vacuum field operators eliminated by the normal and time ordering, the correlation function of Eq. (A11) can be evaluated by defining power operators which represent the interference between the source field and the local oscillator field,

$$\hat{P}_{S;i}(t) \equiv \frac{c}{8\pi} \int d^2\vec{x}_\perp \mathcal{E}^*_{\mathrm{LO};i}(t) \hat{\mathcal{E}}_{S;i}(t). \tag{A15}$$

Then the total power operators which appear in the correlation functions of Eq. (A11) can be written as

$$\begin{aligned} C_{12}(t,t') = \langle :[P_{\mathrm{LO};1} + \hat{P}_{S;1} + \hat{P}^\dagger_{S;1} + \hat{\epsilon}_{SS;1}][P'_{\mathrm{LO};1} + \hat{P}'_{S;1} \\ + \hat{P}^{\dagger\prime}_{S;1} + \hat{\epsilon}'_{SS;1}]: \rangle_Q - \langle :[P_{\mathrm{LO};1} + \hat{P}_{S;1} + \hat{P}^\dagger_{S;1} \\ + \hat{\epsilon}_{SS;1}][P'_{\mathrm{LO};2} + \hat{P}'_{S;2} + \hat{P}^{\dagger\prime}_{S;2} + \hat{\epsilon}'_{SS;2}]: \rangle_Q , \end{aligned} \tag{A16}$$

where the double dots denote that the $\hat{P}_S$ operators are normal and time ordered, as required after elimination of the explicit vacuum field operators. In Eq. (A16), $\hat{\epsilon}_{SS;i}$ is a scattered power operator which is quadratic in the source field operators and which does not contain the local oscillator field.

In the experiments, the driving field, the local oscillator field, and atomic samples are adjusted so that $P_{\mathrm{LO};1}(t) = P_{\mathrm{LO};2}(t)$ and also so that the total power operators satisfy $\langle \hat{P}_1(t) \rangle_Q = \langle \hat{P}_2(t) \rangle_Q$, i.e., signals with identical mean values are obtained from the two samples. This requires

$$\langle \hat{P}_{S;1} + \hat{P}^\dagger_{S;1} + \hat{\epsilon}_{SS;1} \rangle_Q = \langle \hat{P}_{S;2} + \hat{P}^\dagger_{S;2} + \hat{\epsilon}_{SS;2} \rangle_Q , \tag{A17}$$

where the vacuum field operators do not contribute to the average power, and equal LO powers are used. Hence, in Eq. (A16), the seven terms which are quadratic or explicitly linear in P_{LO} in the first correlation function are cancelled by the corresponding seven terms in the second. Further, the remaining terms which are quadratic in $\hat{\epsilon}_{SS}$ are negligible compared to those quadratic in $\hat{P}_S$, as the former operators are not proportional to the local oscillator field, while the later are. The correlation function of Eq. (A16) is therefore simplified to

$$\begin{aligned} C_{12}(t,t') = \langle \hat{P}'_{S;1} \hat{P}_{S;1} \rangle_Q - \langle \hat{P}'_{S;1} \hat{P}_{S;2} \rangle_Q + \langle \hat{P}^\dagger_{S;1} \hat{P}'_{S;1} \rangle_Q \\ - \langle \hat{P}^\dagger_{S;1} \hat{P}'_{S;2} \rangle_Q + \text{c.c.}, \end{aligned} \tag{A18}$$

where the prime denotes evaluation at time t', while the unprimed terms are evaluated at time t. Note the complex conjugate terms are consistent with the normal and time ordering.

Since the operators $\hat{P}_S$ of Eq. (A15) contain only scattered field operators, they can be expanded in terms of the corresponding operators for individual atoms. Hence

$$\hat{P}_{S;i}(t) \equiv \sum_a \hat{P}^{(a)}_S(t), \tag{A19}$$

where the sum is over atoms (a) in a single sample, i. Note that at high density, the driving field can be substantially modified by interaction with the atomic medium, and the atoms can couple to each other via the radiation field. In this case, the correlation function is not necessarily linear in the atomic density. For simplicity, here we will consider only the case of small absorption, where the correlation function is linear in the atomic density, and the atoms radiate independently. Denoting by (a,a') the atoms in sample 1 and by (b,b') the atoms in sample 2, a typical correlation function which appears in Eq. (A18) can be written as

$$\begin{aligned} \langle \hat{P}'_{S;1} \hat{P}_{S;1} \rangle_Q - \langle \hat{P}'_{S;1} \hat{P}_{S;2} \rangle_Q = \sum_{a',a} \langle \hat{P}^{(a')'}_S \hat{P}^{(a)}_S \rangle_Q \\ - \sum_{a',b} \langle \hat{P}^{(a')'}_S \hat{P}^{(b)}_S \rangle_Q , \end{aligned} \tag{A20}$$

where primed operators are evaluated at time t', while unprimed operators are evaluated at time t.

The majority of the terms in Eq. (A20) arise from independent atoms. In the first term there are $N_1(N_1 - 1)$ contributions for $a \neq a'$, and in the second, which arises from independent samples, there are $N_1 N_2$ contributions with $b \neq a'$. Now independent atoms, which traverse a given local oscillator field, arrive at random times relative to one another. For stable classical driving fields, these terms make τ-independent contributions to the correlation function, Eq. (A3). Therefore, they do not contribute to the spectrum for $\omega > 0$, and they may be dropped, yielding only the sum in the first term with $a' = a$. Since each atom is correlated with itself, this yields the desired atom noise spectrum. Due to technical noise, however, there are additional correlations in the independent-atom terms.

To take into account the effects of classical fluctuations on the correlation functions, it is convenient to write the scattered power operators in the form

$$\hat{P}^{(a)}_S \rightarrow \hat{P}^{(a)}_S + \delta P^{(a)}_S ,$$

where the first term denotes the single atom power operator for stable classical driving and LO fields, and the second term denotes the classical fluctuation in the mean scattered power per atom which is due to technical noise in either the LO or driving fields.

Since the classical fluctuation has a zero mean value, and is independent of $\hat{P}_S^{(a)}$, the correlation function [Eq. (A20)], can be written in the form

$$\langle \hat{P}'_{S;1}\hat{P}_{S;1}\rangle_Q - \langle \hat{P}'_{S;1}\hat{P}_{S;2}\rangle_Q = \sum_a \langle \hat{P}_S^{(a)\prime}\hat{P}_S^{(a)}\rangle_Q + \sum_{a',a} \langle \delta P_S^{(a')\prime}\delta P_S^{(a)}\rangle_Q - \sum_{a',b} \langle \delta P_S^{(a')\prime}\delta P_S^{(b)}\rangle_Q . \tag{A21}$$

Here τ-independent contributions have been dropped, and the first term in Eq. (A21) contains only the sum of single-atom contributions, i.e., $a'=a$, neglecting classical fluctuations. Since each atom is correlated with itself, these yield the dominant noise contribution to the spectrum. Now, the last two terms in Eq. (A21), which involve primarily independent atoms, only contain correlations that arise from fluctuations in the driving and local oscillator fields. The first of these terms is proportional to the square of the number of atoms in sample 1, i.e., to N_1^2, while the second is proportional to N_1N_2. If the local oscillator and driving fields are derived from a common source, the classical noise in the two samples can be made nearly identical by arranging for both samples to have the approximately the same number of atoms, i.e., $N_1=N_2$. In this case, the last two terms of Eq. (A21) are subtracted, leaving only the first term. The correlation function of Eq. (A21) then takes the form of a sum of single atom contributions, and Eq. (A18) yields

$$C_{12}(t,t') = \sum_a \langle \hat{P}_S^{(a)\prime}\hat{P}_S^{(a)}\rangle_Q + \sum_a \langle \hat{P}_S^{\dagger(a)}\hat{P}_S^{(a)\prime}\rangle_Q + \text{c.c.} \tag{A22}$$

When the local oscillator powers in the two interaction regions are well balanced, i.e., so that the noise spectrum is dominated by the LO shot noise in the absence of atoms, but the number of atoms in the first and second interaction regions differs by ΔN, then the technical noise contribution to the atom quadrature noise spectra is suppressed by a factor of order $\Delta N/N$, compared to that which would be obtained using balanced homodyne detection with a beam splitter.

In Eq. (A22), the first term and its complex conjugate will yield contributions to the noise spectrum which depend on the relative phase between the local oscillator and driving fields. The second term and its complex conjugate will yield phase-independent contributions.

APPENDIX B: POWER AUTOCORRELATION FUNCTION

In this section, the power autocorrelation function, $C(t,t')$, of Eq. (A10) is determined by calculating the normal and time-ordered power autocorrelation function, $C_{12}(t,t')$ of Eq. (A22) for a thin sample. This is accomplished by writing the scattered field operator, which appears in Eq. (A15), in terms of the Bloch vector operators for the individual atoms.

1. Scattered power operator

We assume that the LO and driving fields propagate nominally in the **y** direction (Fig. 3). Since the local oscillator is highly collimated, the required overlap integral between the local oscillator and the scattered field may be calculated using a paraxial approximation. Hence the local oscillator field in the detector plane, y_D, is related to that in the source plane, y', according to

$$\vec{\mathcal{E}}_{\rm LO}(y_D,\vec{x}_\perp,t) = \int dt'\,d^2\vec{x}'_\perp\, g(y_D-y',\vec{x}_\perp-\vec{x}'_\perp,t-t') \times \vec{\mathcal{E}}_{\rm LO}(y',\vec{x}'_\perp,t'), \tag{B1}$$

and $q=2\pi/\lambda$ is the optical wave vector. The Green's function in the paraxial approximation is given by

$$g(\vec{x}-\vec{x}',t-t') = \Theta(y-y')\,\delta\!\left(t-t'-\frac{y-y'}{c}\right) \times \frac{q}{2\pi i(y-y')} e^{i[q(\vec{x}_\perp-\vec{x}'_\perp)^2/2(y-y')]}. \tag{B2}$$

The projection of the scattered field operator onto the polarization vector of the LO at position $\vec{x}$ in the LO beam is defined as $\hat{\mathcal{E}}_S(\vec{x},t)\equiv\hat{e}^*_{\rm LO}\cdot\vec{\mathcal{E}}_S(\vec{x},t)$. It is given in terms of the slowly varying atomic polarization operator at the source, $\hat{\mathcal{P}}(\vec{x}',t')=\hat{e}^*_{\rm LO}\cdot\vec{\mathcal{P}}(\vec{x}',t')$, where the LO field vector and the atomic polarization vector contain no components along $\hat{y}$:

$$\hat{\mathcal{E}}_S(y_D,\vec{x}_\perp,t) = 2\pi i q\int dt'\,d^3\vec{x}'\, g(y_D-y',\vec{x}_\perp-\vec{x}'_\perp,t-t') \times \hat{\mathcal{P}}(y',\vec{x}'_\perp,t'). \tag{B3}$$

Using Eqs. (B3) and (B2) in Eq. (A15) for the scattered power operator, one obtains

$$\hat{P}_S(t) = \frac{c}{8\pi}2\pi i q\int d^3\vec{x}'\,\mathcal{E}^*_{\rm LO}(\vec{x}'_\perp)\hat{\mathcal{P}}(\vec{x}',t'_{\rm ret}), \tag{B4}$$

where $t'_{\rm ret}\simeq t-y_D/c$, assuming that the source is small enough that y'/c is short compared to the relevant time scales for the system. Since the time can be uniformly shifted in the correlation function, we take $t'_{\rm ret}=t$. Note that Eq. (B4) yields the same power as would be obtained by interfering the LO field with a scattered field $2\pi i q\int dz'\mathcal{P}$. This is a consequence of power conservation: the overlap integral must be the same for any transverse plane after the medium.

The dipole polarization per unit volume, $\vec{P}$, can be related to the Bloch vector components in the Heisenberg picture. Defining $\hat{\rho}$ as the atomic density operator, and $\vec{\mathcal{P}}$ as the slowly varying polarization operator, we have

$$\vec{P}(\vec{x},t)=\tfrac{1}{2}\vec{\mathcal{P}}(\vec{x},t)e^{iqy-i\Omega t}+\text{c.c.}$$

$$=\sum_a \vec{\mu}_{01}\hat{\rho}_{10}^{(a)}[\vec{x}_a(t),t]\delta[\vec{x}-\vec{x}_a(t)]+\text{H.c.}, \quad \text{(B5)}$$

where Ω is the laser frequency and $q=\Omega/c$ is the optical wave vector. Here $|1\rangle$ denotes the atomic excited state, $|0\rangle$ denotes the ground state. (a) denotes the contribution of atom (a), which travels along a straight line trajectory in the atomic beam, $\vec{x}_a(t)$. Hence $\hat{\mathcal{P}}=\hat{e}_{\rm LO}^{*}\cdot\vec{\mathcal{P}}$ is given by

$$\hat{\mathcal{P}}(\vec{x},t)=2\hat{e}_{\rm LO}^{*}\cdot\vec{\mu}_{01}\sum_a \hat{\rho}_{10}^{(a)}[\vec{x}_a(t),t]\delta[\vec{x}-\vec{x}_a(t)]e^{-iqy+i\Omega t}. \quad \text{(B6)}$$

The single-atom density-matrix operator can be written in terms of the slowly varying density matrix operator $\hat{\sigma}_{10}$ as

$$\hat{\rho}_{10}^{(a)}(t)\equiv\hat{\sigma}_{10}[\vec{x}_a(t),t]e^{iqy^{(a)}(t)-i\Omega t}. \quad \text{(B7)}$$

Then Eq. (B4) can be rewritten in the form of single-atom contributions, as in Eq. (A19),

$$\hat{P}_S(t)=\sum_a \hat{P}_S^{(a)}(t), \quad \text{(B8)}$$

where

$$\hat{P}_S^{(a)}(t)=i\frac{\hbar\Omega}{2}\beta_{\rm LO}^{*}[\vec{x}_a(t)]\hat{\sigma}_{10}^{(a)}[\vec{x}_a(t),t]. \quad \text{(B9)}$$

Here, the effective Rabi frequency of the LO is defined as

$$\beta_{\rm LO}(\vec{x}_a)=\frac{\hat{e}_{\rm LO}\cdot\vec{\mu}_{10}}{\hbar}\mathcal{E}_{\rm LO}[\Theta(x_a+a/2)-\Theta(x_a-a/2)]e^{-z_a^2/b^2}$$

$$\equiv|\beta_{\rm LO}(\vec{x}_a)|e^{i\phi_{\rm LO}}, \quad \text{(B10)}$$

where $\Theta(x)$ is a unit step function. The LO and driving fields are taken to have rectangular profiles of full width a along the atomic beam axis, **x**, to simplify calculations of the atomic dipole operator in the off-resonant case, as described below. In the z direction (see Fig. 3), the fields are taken to have Gaussian profiles of $1/e$ radius b. For simplicity, we suppress the z argument in the following.

2. Dipole operator

The single-atom scattered power operator, Eq. (B9), can be used to evaluate the correlation function given by Eq. (A22) in terms of the atomic dipole autocorrelation function. This is accomplished by finding the Heisenberg equations of motion for the slowly varying density operator $\hat{\sigma}$, which is defined by Eq. (B7). We assume in the following that the atom has a long radiative lifetime compared to the transit time across the laser interaction region. In this case, at most one spontaneous photon is emitted per atom, and the driving field can be treated as a strong classical field in determining atomic Heisenberg operators to zeroth order in the vacuum field, which is all that is needed for evaluation of the normal and time-ordered correlation functions for a thin sample.

Since the magnetically compensated supersonic beam effectively cancels the Doppler shifts due to atomic motion along the laser beam propagation direction **y** (Fig. 3), we assume for simplicity that Doppler broadening can be neglected, and take $v_y=0$. Also, we assume that atoms which cross the laser fields move negligibly in the vertical **z** direction. Hence we take the atoms to move only in the **x** direction. The atom position in the source, x', at time t', then can be written in terms of the position of the atom, x, at time t as $x'(t')=x-v_x(t-t')$, so that the interaction potential as seen in the atom frame can be taken as

$$V(t')=-\vec{\mu}\cdot\vec{E}_p[x-v_x(t-t'),y',z',t']. \quad \text{(B11)}$$

In the following, we take t to be a fixed time, and let t' be the time variable in the evolution equations. Our prescription will be to determine the evolution of the Heisenberg operators from the time $t'=0$, when the Heisenberg and Schrödinger operators are taken to coincide, to the time $t'=t$, when the atom is at position x in the driving laser beam.

The driving field can be written as

$$\vec{E}_p(\vec{x}',t')=\tfrac{1}{2}\hat{e}_p\mathcal{E}_p(x',z')e^{i(qy'-\Omega t')}+\text{c.c.} \quad \text{(B12)}$$

The corresponding driving field Rabi frequency is then defined by

$$\beta_p(x')\equiv\frac{\vec{\mu}_{10}\cdot\hat{e}_p}{\hbar}\mathcal{E}_p(x'), \quad \text{(B13)}$$

where the z' argument is suppressed, since it is time independent by assumption, i.e., $z'=z$ as in Eq. (B10).

Using Eq. (B11) for the interaction, one obtains the effective Hamiltonian in the Schrödinger picture (S) as

$$\hat{H}^S(t')=\hbar\omega_o|1\rangle\langle 1|-\frac{\hbar}{2}\{\beta_p[x-v_x(t-t')]$$

$$\times e^{i(qy-\Omega t')}|1\rangle\langle 0|+\text{H.c.}\}. \quad \text{(B14)}$$

In writing Eq. (B14), we assumed $y'\simeq y$ and $z'\simeq z$.

To find the Heisenberg equations of motion for the slowly varying density operator, let the Schrödinger picture density (pseudospin) operators be defined by

$$\begin{aligned}\hat{\sigma}_{10}^S&\equiv|0\rangle\langle 1|,\\ \hat{\sigma}_{01}^S&\equiv|1\rangle\langle 0|,\\ \hat{\sigma}_{11}^S&\equiv|1\rangle\langle 1|,\\ \hat{\sigma}_{00}^S&\equiv|0\rangle\langle 0|.\end{aligned} \quad \text{(B15)}$$

Equations (B15) are defined so that $\langle\psi(t)|\hat{\sigma}_{10}^S|\psi(t)\rangle=\langle\psi(t)|0\rangle\langle 1|\psi(t)\rangle=A_0^{*}A_1=\rho_{10}(t)$, as desired, with A_i a Schrödinger picture amplitude and ρ_{10} the corresponding density-matrix element.

The density operators in the Heisenberg picture, and the corresponding slowly varying density operators, $\hat{\sigma}_{ij}(t')$, are defined by

$$\hat{\rho}^H_{10}(t') \equiv \hat{U}^\dagger(t')\hat{\sigma}^S_{10}\hat{U}(t') \equiv \hat{\sigma}_{10}(t')e^{iqy-i\Omega t'}, \qquad \hat{\rho}^H_{ii}(t') \equiv \hat{U}^\dagger(t')\hat{\sigma}^S_{ii}\hat{U}(t') \equiv \hat{\sigma}_{ii}(t'), \tag{B16}$$

where $i=0$ and 1. Here the time translation operator obeys

$$\dot{\hat{U}}(t') = -\frac{i}{\hbar}\hat{H}^S(t')\hat{U}(t'). \tag{B17}$$

Equations (B16), (B17), and (B14) yield the Heisenberg equations of motion for the slowly varying density operators:

$$\dot{\hat{\sigma}}_{10}(t') - i(\Omega-\omega_o)\hat{\sigma}_{10}(t') = -i\frac{\beta_p(t')}{2}[\hat{\sigma}_{11}(t')-\hat{\sigma}_{00}(t')],$$

$$\dot{\hat{\sigma}}_{11}(t') = i\frac{\beta_p(t')}{2}\hat{\sigma}_{01}(t') + \text{H.c.}, \qquad \dot{\hat{\sigma}}_{00}(t') = -\dot{\hat{\sigma}}_{11}(t'), \tag{B18}$$

where

$$\beta_p(t') = \beta_p[x - v_x(t-t')] \equiv e^{i\phi_p}|\beta_p(t')| \tag{B19}$$

and $\beta_p(x')$, is given by Eq. (B13). Here ϕ_p is a time-independent driving field phase.

It is convenient to define the Bloch vector component operators, $\hat{x}$, $\hat{y}$, and $\hat{z}$ in terms of the slowly varying density operators, σ_{ij}:

$$\hat{z}(t') \equiv \tfrac{1}{2}[\hat{\sigma}_{11}(t')-\hat{\sigma}_{00}(t')], \qquad \hat{\sigma}_{10}(t') \equiv e^{i\phi_p}[\hat{x}(t')-i\hat{y}(t')]. \tag{B20}$$

Equations of motion for the Bloch vector component operators are readily found from Eqs. (B18),

$$\dot{\hat{x}}(t') - \Delta\hat{y}(t') = 0, \qquad \dot{\hat{y}}(t') + \Delta\hat{x}(t') = |\beta_p(t')|\hat{z}(t'), \qquad \dot{\hat{z}}(t') = -|\beta_p(t')|\hat{y}(t'). \tag{B21}$$

To solve Eqs. (B21) for the case of nonzero detuning, it is convenient to assume that the laser beam has a rectangular profile along the atomic beam propagation direction **x**, as assumed in Eq. (B10). The initial conditions are determined from the Heisenberg operators, Eq. (B16), at $t'=0$, i.e.,

$$\hat{\sigma}_{10}(t'=0) = \hat{\sigma}^S_{10}e^{-iqy},$$

and $\sigma_{ii}(t'=0)=\sigma^S_{ii}$. Then with the definition

$$\phi'_p \equiv \phi_p + qy, \tag{B22}$$

the initial conditions are

$$\hat{x}(t'=0) = \tfrac{1}{2}e^{-i\phi'_p}\hat{\sigma}^S_- + \text{H.c.}, \qquad \hat{y}(t'=0) = \frac{1}{2i}e^{i\phi'_p}\hat{\sigma}^S_+ + \text{H.c.}, \qquad \hat{z}(t'=0) = \tfrac{1}{2}[\hat{\sigma}^S_{11}-\hat{\sigma}^S_{00}]. \tag{B23}$$

Here, $\hat{\sigma}^S_- \equiv \hat{\sigma}^S_{10} = |0\rangle\langle 1|$, according to Eq. (B15) and $\hat{\sigma}^S_+$ is its adjoint.

For a rectangular pump beam of width a, the Rabi frequency is given by

$$|\beta_p(t')| = |\beta_p[x' = x - v_x(t-t')]| = |\beta_p|\left[\Theta\left(x'+\frac{a}{2}\right)-\Theta\left(x'-\frac{a}{2}\right)\right]e^{-(z^2/b^2)}, \tag{B24}$$

where $\Theta(x)$ is a unit step function, and b is the driving field $1/e$ radius in the vertical **z** direction (Fig. 1). We assume that the time, $t \gg a/v_x$, so that the atom is far to the left of the driving field at $t'=0$. For simplicity, the $z'=z$ dependence of the Rabi frequency is suppressed in the following.

We note that an atom which is at position x at time t arrives at the position $x'=-a/2$, where the driving field starts, at time $t'=t-(x+a/2)/v_x$. Hence the atoms evolve freely from $t'=0$ to $t'=t-(x+a/2)/v_x$. For completeness, the free evolution will be determined here to show that its only effect on the initial conditions in the interaction region is to introduce an invariant phase shift $\varphi(t-x/v_x)$ in the coefficients of $\sigma^S_\pm$. This is as one would expect. To find the Heisenberg Bloch vector operators at the time the atom arrives at the left side of the driving field, $x'=-a/2$, Eqs. (B21) are solved with $|\beta_p|=0$ to obtain

$$(\hat{x}-i\hat{y})(t') = (\hat{x}-i\hat{y})(t'=0)e^{i\Delta t'},$$

and $\hat{z}(t')=\hat{z}(t'=0)$. For $t'=t-(x+a/2)/v_x$, one obtains with the initial conditions [Eqs. (B23)],

$$\hat{z}[t-(x+a/2)/v_x] = \frac{\hat{\sigma}^S_{11}-\hat{\sigma}^S_{00}}{2},$$

$$\hat{x}[t-(x+a/2)/v_x] = \frac{\hat{\sigma}^S_-}{2}e^{-i\phi'_p+i\Delta[t-(x+a/2)/v_x]} + \text{H.c.}, \qquad \hat{y}[t-(x+a/2)/v_x] = i\frac{\hat{\sigma}^S_-}{2}e^{-i\phi'_p+i\Delta[t-(x+a/2)/v_x]} + \text{H.c.} \tag{B25}$$

The atom travels across the driving field (from $x'=-a/2$ to $x'=a/2$) during the time interval $t'=t-(x+a/2)/v_x$ to $t'=t-(x-a/2)/v_x$. To find the Heisenberg Bloch vector operators in this time interval, Eqs. (B21) are solved for the case $|\beta_p|=\text{const}$. For this purpose, it is convenient to define a time τ', which is the time relative to the time the atom arrives at $x'=-a/2$, i.e.,

$$\tau' \equiv t' - [t-(x+a/2)/v_x]. \tag{B26}$$

Hence $\tau'=0$ corresponds to the initial conditions on the Heisenberg operators at $t'=t-(x+a/2)/v_x$, when the atom arrives at the input side of the pump beam, i.e., Eqs. (B25).

With $dt'=d\tau'$, and the overdot representing differentiation with respect to τ' in Eqs. (B21), one obtains by direct differentiation an equation of motion for $\hat{y}(\tau')$,

$$\ddot{\hat{y}}+\beta'^2\,\hat{y}=0, \tag{B27}$$

where the generalized Rabi frequency is defined by

$$\beta'\equiv\beta'(z)=\sqrt{\Delta^2+\beta_p(z)^2}. \tag{B28}$$

Here we include the vertical z dependence of the pump beam field, which will be taken to be Gaussian. Note that $z'=z$ is assumed, since we neglect the motion perpendicular to **x**, as discussed above.

Equation (B27) is readily solved using Eqs. (B21) to obtain $\dot{\hat{y}}(\tau'=0)$,

$$\hat{y}(\tau')=-\hat{x}(\tau'=0)\frac{\Delta}{\beta'}\sin\beta'\tau'+\hat{y}(\tau'=0)\cos\beta'\tau' +\hat{z}(\tau'=0)\frac{|\beta_p|}{\beta'}\sin\beta'\tau'. \tag{B29}$$

The other Bloch vector operators then are obtained from Eqs. (B21),

$$\hat{x}(\tau')=\hat{x}(\tau'=0)+\Delta\int_0^{\tau'}d\tau''\hat{y}(\tau''),$$

which yields

$$\hat{x}(\tau')=\hat{x}(\tau'=0)\left[\frac{|\beta_p|^2}{\beta'^2}+\frac{\Delta^2}{\beta'^2}\cos\beta'\tau'\right]+\hat{y}(\tau'=0)\frac{\Delta}{\beta'} \times\sin\beta'\tau'+\hat{z}(\tau'=0)\frac{|\beta_p|\Delta}{\beta'^2}(1-\cos\beta'\tau'), \tag{B30}$$

and from

$$\hat{z}(\tau')=\hat{z}(\tau'=0)-|\beta_p|\int_0^{\tau'}d\tau''\hat{y}(\tau''),$$

which yields

$$\hat{z}(\tau')=\frac{|\beta_p|\Delta}{\beta'^2}(1-\cos\beta'\tau')\hat{x}(\tau'=0) -\frac{|\beta_p|}{\beta'}\sin\beta'\tau'\hat{y}(\tau'=0) +\left[\frac{\Delta^2}{\beta'^2}+\frac{|\beta_p|^2}{\beta'^2}\cos\beta'\tau'\right]\hat{z}(\tau'=0). \tag{B31}$$

Equations (B29), (B30), and (B31) are valid in the time interval, $t-(x+a/2)/v_x\leq t'\leq t-(x-a/2)/v_x$. Hence these solutions can be multipled by a factor $\Theta[t'-t+(x+a/2)/v_x]-\Theta[t'-t+(x-a/2)/v_x]$, to appropriately restrict the range of t'.

We are interested in the Heisenberg operators at time $t'=t$, when the atom arrives at position x. At $t'=t$, Eq. (B26) shows that $\tau'=(x+a/2)/v_x$. Using Eq. (B20) and the above restriction factor yields

$$\hat{\sigma}_{10}(t'=t)=[\Theta(x+a/2)-\Theta(x-a/2)]e^{i\phi_p} \times\left[\hat{x}\left(\tau'=\frac{x+a/2}{v_x}\right)-i\hat{y}\left(\tau'=\frac{x+a/2}{v_x}\right)\right]. \tag{B32}$$

The solution is conveniently written in terms of the effective pulse area

$$\theta_e\equiv\theta_e(x,z)\equiv\beta'(z)\frac{x+a/2}{v_x},\quad |x|\leq\frac{a}{2}. \tag{B33}$$

Using the initial conditions at $\tau'=0$, Eqs. (B25), after some algebra we obtain

$$\hat{\sigma}_{10}(t'=t)=[\Theta(x+a/2)-\Theta(x-a/2)]\left\{\frac{\hat{\sigma}_-^S}{2}e^{i\varphi}\left[\frac{|\beta_p|^2}{\beta'^2} +\left(1+\frac{\Delta^2}{\beta'^2}\right)\cos\theta_e+\frac{2i\Delta}{\beta'}\sin\theta_e\right] +\frac{\hat{\sigma}_+^S}{2}e^{2i\phi_p-i\varphi}\frac{|\beta_p|^2}{\beta'^2}(1-\cos\theta_e) -i\frac{\hat{\sigma}_{11}^S-\hat{\sigma}_{00}^S}{2}e^{i\phi_p}\left[\frac{|\beta_p|}{\beta'}\sin\theta_e +i\frac{|\beta_p|\Delta}{\beta'^2}(1-\cos\theta_e)\right]\right\}, \tag{B34}$$

where $\varphi\equiv\Delta[t-(x+a/2)/v_x]-qy$.

The single atom scattered power operator is readily evaluated from Eq. (B9) using Eq. (B34) and the effective Rabi frequency of the local oscillator, Eq. (B10),

$$\hat{P}_S^{(a)}(t)=\frac{\hbar\Omega}{2}|\beta_{\rm LO}(x,z)|e^{-i\phi_{\rm LO}}\left\{\frac{\hat{\sigma}_{11}^S-\hat{\sigma}_{00}^S}{2}e^{i\phi_p}\left[\frac{|\beta_p|}{\beta'}\sin\theta_e +i\frac{|\beta_p|\Delta}{\beta'^2}(1-\cos\theta_e)\right]+i\frac{\hat{\sigma}_-^S}{2}e^{i\varphi} \times\left[\frac{|\beta_p|^2}{\beta'^2}+\left(1+\frac{\Delta^2}{\beta'^2}\right)\cos\theta_e+\frac{2i\Delta}{\beta'}\sin\theta_e\right] +i\frac{\hat{\sigma}_+^S}{2}e^{2i\phi_p-i\varphi}\frac{|\beta_p|^2}{\beta'^2}(1-\cos\theta_e)\right\}, \tag{B35}$$

where Eq. (B10) shows that $\beta_{\rm LO}(x,z)$ is nonzero only in the interval $|x|\leq a/2$, so that the step functions of Eq. (B34) are implicitly included.

3. Power autocorrelation function

The power autocorrelation function of Eq. (A22) requires the evaluation of two single-atom correlation functions, which take the form $\langle \hat{P}_S^{(a)}(t+\tau)\hat{P}_S^{(a)}(t)\rangle$ and $\langle \hat{P}_S^{(a)\dagger}(t+\tau)\hat{P}_S^{(a)}(t)\rangle$. In evaluating these single-atom correlation functions, we require $t'=t$ in one factor, which yields Eq. (B35). For the second factor, we require $t'=t+\tau$ which increases τ' of Eqs. (B29), (B30), and (B31) by τ. This is equivalent to changing the effective pulse area of Eq. (B33) by $x\rightarrow x+v_x\tau$ [see Eq. (B9)]. Since $x\equiv x(t)$ labels a given atom by its position at time t, the phase $\varphi=\varphi(x-v_x t)$ which appears in Eqs. (B34) and (B35) is therefore invariant and can be treated as a constant. Alternatively, one can make the combined substitutions $t\rightarrow t+\tau$ and $x(t)\rightarrow x(t+\tau)=x+v_x\tau$ ($y\rightarrow y$ for $v_y=0$), i.e., a given atom is equally well labelled by its position at time t or at time $t+\tau$. Again the phase φ which appears in Eq. (B34) is invariant. Note that for the case $v_y\neq 0$, the phase $qy\rightarrow q(y-v_y t)$ also is invariant.

For the case where all atoms are initially in the ground state, $|0\rangle$, $\hat{\sigma}_{00}^S|0\rangle=1|0\rangle$, and $\langle 0|\hat{\sigma}_-^S\hat{\sigma}_+^S|0\rangle=1$ make the only nonzero contributions to the power autocorrelation functions. It is straightforward to obtain

$$\langle \hat{P}_S^{(a)\dagger}(t+\tau)\hat{P}_S^{(a)}(t)\rangle+\text{c.c.} = \frac{(\hbar\Omega)^2}{8}|\beta_{\text{LO}}(x,z)||\beta_{\text{LO}}(x+v_x\tau)| \times\left(\frac{|\beta_p|}{\beta'}\right)^2[\sin\theta_e'\,\sin\theta_e+(1-\cos\theta_e)(1-\cos\theta_e')], \tag{B36}$$

where $\theta_e'\equiv\theta_e(x+v_x\tau,z)$ and θ_e is given by Eq. (B33). For $\tau\geqslant 0$, we have

$$\langle \hat{P}_S^{(a)}(t+\tau)\hat{P}_S^{(a)}(t)\rangle+\text{c.c.} = \frac{(\hbar\Omega)^2}{8}|\beta_{\text{LO}}(x,z)||\beta_{\text{LO}}(x+v_x\tau,z)|\left(\frac{|\beta_p|}{\beta'}\right)^2 \times\left\{[\sin\theta_e'\sin\theta_e-(1+\cos\theta_e')(1-\cos\theta_e)]\cos 2\phi + \frac{\Delta}{\beta'}[\sin\theta_e(1-\cos\theta_e')-\sin\theta_e'(1-\cos\theta_e)]\sin 2\phi\right\}, \tag{B37}$$

where $\phi\equiv\phi_{\text{LO}}-\phi_p$ is the relative phase between the LO and driving fields.

The correlation function C_{12} of Eq. (A22) consists of a sum of terms, one for each atom, which take the form of Eqs. (B36) and (B37). Since all atoms are equivalent, and labelled by their position x at time t, the sum can be replaced by an integral over the atomic density, n, with $n\,dx\,dz\,dy$ the number of atoms at x. The integral $\int dy=L$, where L is the sample length. Further, for identical samples, the correlation functions C_{12} and C_{21} appearing in Eq. (A10) are identical, so that $C_{12}+C_{21}=2\,C_{12}$. Hence the atom contribution to the one sided power spectrum, Eq. (A12), takes the form

$$S_{\text{ATOM}}(\omega)=2\,\text{Re}\int_0^\infty d\tau\frac{e^{i\omega\tau}}{\pi}2\int n\,dx\,dy\,dz[\langle \hat{P}_S^{(a)\dagger}(t+\tau) \times\hat{P}_S^{(a)}(t)\rangle+\langle \hat{P}_S^{(a)}(t+\tau)\hat{P}_S^{(a)}(t)\rangle+\text{c.c.}] \tag{B38}$$

It is convenient to denote the atom transit time across the driving or LO fields by

$$\tau_o\equiv a/v_x. \tag{B39}$$

Further, an effective number of atoms per second crossing one interaction region can be defined as

$$\dot{N}\equiv n\sqrt{\pi}v_x bL. \tag{B40}$$

Note that a factor of $\sqrt{\pi}$ is incorporated, since the beam is assumed to be Gaussian in the vertical direction with b the field $1/e$ width. Finally, the maximum pulse area is defined as

$$\theta_M\equiv\beta_p\tau_o. \tag{B41}$$

Note that the beam is assumed to have a square profile of full width a along $\mathbf{x}$, so that no $\sqrt{\pi}$ is used here.

The power spectrum, Eq. (B38), can be written as an integral over dimensionless variables with the substitutions $\tau=\tilde{\tau}\tau_o$, $z=\eta b$, and $x=\xi a$. Equation (B10) shows that $\beta_{\text{LO}}(\xi,\eta)\propto[\Theta(\xi+\frac{1}{2})-\Theta(\xi-\frac{1}{2})]$. Hence to evaluate the atom contributions to the power spectrum, we require integrals of the form

$$I(\omega)=2\,\text{Re}\int_0^\infty d\tilde{\tau}\,e^{-i\omega\tau_o\tilde{\tau}}\int_{-\infty}^\infty d\xi[\Theta(\xi+\tfrac{1}{2})-\Theta(\xi-\tfrac{1}{2})] \times[\Theta(\xi+\tfrac{1}{2}+\tilde{\tau})-\Theta(\xi-\tfrac{1}{2}+\tilde{\tau})]f(\xi)g(\xi+\tilde{\tau}), \tag{B42}$$

where f and g are functions of ξ and η, as given by Eqs. (B36) and (B37). The product of the two Θ functions have a nonzero overlap for $-\frac{1}{2}\leqslant\xi\leqslant\frac{1}{2}-\tilde{\tau}$. Hence, the maximum value of $\tilde{\tau}=1$.

With these results, the phase-dependent power spectrum $S(\nu,\phi)\Delta\nu\equiv S_{\Delta P}(\omega)2\pi\Delta\nu$ is obtained from Eq. (A12), where ν ($\Delta\nu$) denotes the spectrum analyzer frequency (bandwidth) in Hz and $\phi\equiv\phi_{\text{LO}}-\phi_p$ is the relative phase between the local oscillator and driving fields. This can be written in terms of distinct noise sources,

$$S(\nu,\phi)=\eta_S\left[P+\dot{N}\hbar\Omega\left(\frac{P_{\text{LO}}}{2P_p}\right)\frac{\eta_o}{4}\theta_M^2\{[F_D(\nu)+F_{\text{SP}}(\nu)] +[F_D(\nu)+F_B(\nu)]\cos 2\phi+F_N(\nu)\sin 2\phi\}\right]. \tag{B43}$$

In Eq. (B43), we have used $|\beta_{\rm LO}/\beta_p|^2 = P_{\rm LO}/(2\,P_p)$ for a blocking polarizer at 45° in the **x**-**z** plane. The first term in Eq. (B43) is the mean-square shot noise due to the total transmitted power from both regions, including the mean absorption, i.e., $P = P_1 + P_2$. Here $\eta_S \equiv 2\hbar\Omega\,\eta_o \Delta\nu$, with η_o the detection system efficiency.

The spectral functions, $F_i(\nu)$, which appear in Eq. (B43) can be written in terms of normal and time-ordered correlation functions for $\tilde{\tau} \geqslant 0$, with the definitions

$$F[\,f(\theta),g(\theta);\nu] = 2\,\mathrm{Re}\int_0^1 d\tilde{\tau}\; e^{-i2\pi\nu\tau_o\tilde{\tau}} C[\,f(\theta),g(\theta);\tilde{\tau}], \tag{B44}$$

where

$$C[\,f(\theta),g(\theta);\tilde{\tau}] = \int_{-\infty}^{\infty}\frac{d\eta}{\sqrt{\pi}} e^{-2\eta^2}\int_{-(1/2)}^{(1/2)-\tilde{\tau}} d\xi\;\frac{\theta_M^2 \mathrm{e}^{-2\eta^2}}{\theta_M'^2(\eta)} \times f[\,\theta(\xi+\tilde{\tau},\eta)]\,g[\,\theta(\xi,\eta)]. \tag{B45}$$

The position-dependent effective Bloch angle is given by

$$\theta(\xi,\eta) = \theta_M'(\eta)\left(\frac{1}{2}+\xi\right), \tag{B46}$$

with the effective maximum pulse area

$$\theta_M'(\eta) \equiv \sqrt{\theta_M^2 \exp(-2\eta^2) + (\Delta\tau_o)^2}. \tag{B47}$$

In Eq. (B45), note that the left argument f is evaluated at a later time, $\xi+\tilde{\tau}$, than the right argument g, which is evaluated at ξ.

With these definitions, we find

$$\begin{aligned} F_D(\nu) &= F[\sin\theta,\sin\theta;\nu], \\ F_{\rm SP}(\nu) &= F[1-\cos\theta,1-\cos\theta;\nu], \\ F_B(\nu) &= F[\cos\theta+1,\cos\theta-1;\nu], \\ F_N(\nu) &= \Delta\tau_o\left\{F\left[1-\cos\theta,\frac{\sin\theta}{\theta_M'}\right] - F\left[\frac{\sin\theta}{\theta_M'},1-\cos\theta\right]\right\}. \end{aligned} \tag{B48}$$

Note that the frequency distributions are determined by Fourier transformation of single-atom correlation functions with respect to ξ, i.e., along the **x** direction, and that the single-atom contributions to the power spectra from different atoms are then summed (integrated) over η in the vertical **z** direction.

For completeness, we also give the phase-dependent absorption as a function of driving field frequency. This is just the expectation value of the single-atom power operator, $P_S^{(a)}(t)$ of Eq. (B35), integrated over the atomic volume, as was done to obtain Eq. (B43). The total power absorbed from *both* regions is given by

$$P_{\rm ABS} = -\dot{N}\hbar\Omega\sqrt{\frac{P_{\rm LO}}{2P_x}}[F_c(\theta_M)\cos\phi + F_s(\theta_M)\sin\phi], \tag{B49}$$

where $\dot{N}$ is the number of atoms per second crossing one region. Here the coefficients F_c and F_s are

$$\begin{aligned} F_c(\theta_M) &= \int_{-\infty}^{\infty}\frac{d\eta}{\sqrt{\pi}} e^{-2\eta^2}\frac{\theta_M^2}{\theta_M'^2}(1-\cos\theta_M'), \\ F_s(\theta_M) &= \int_{-\infty}^{\infty}\frac{d\eta}{\sqrt{\pi}} e^{-2\eta^2}\frac{\theta_M^2}{\theta_M'^2}\frac{\Delta\tau_o}{\theta_M'}(\theta_M'-\sin\theta_M'). \end{aligned} \tag{B50}$$

[1] W. Heitler, *The Quantum Theory of Radiation* (Clarendon, Oxford, 1954).
[2] M. C. Newstein, Phys. Rev. **167**, 89 (1968).
[3] B. R. Mollow, Phys. Rev. **188**, 1969 (1969).
[4] F. Schuda, C. R. Stroud, Jr., and M. Hercher, J. Phys. B **7**, L198 (1974).
[5] W. Hartig, W. Rasmussen, R. Schieder, and H. Walther, Z. Phys. A **278**, 205 (1976).
[6] F. Y. Wu, R. E. Grove, and S. Ezekiel, Phys. Rev. Lett. **35**, 1426 (1975).
[7] H. M. Gibbs and T. N. C. Venkatesan, Opt. Commun. **17**, 87 (1976).
[8] B. R. Mollow, Phys. Rev. A **12**, 1919 (1975).
[9] V. J. Herrman, K.-E. Süsse, and D. Welsch, Ann. Phys. (Leipzig) **30**, 37 (1973).
[10] G. S. Agarwal, *Quantum Statistical Theories of Spontaneous Emission and Their Relation to Other Approaches*, Springer Tracts in Modern Physics Vol. 70 (Springer, Heidelberg, 1974).
[11] S. S. Hassan and R. K. Bullough, J. Phys. B **8**, L147 (1975).
[12] M. E. Smithers and H. S. Freedhoff, J. Phys. B **7**, L432 (1974).
[13] H. J. Carmichael and D. F. Walls, J. Phys. B **8**, L77 (1975); **9**, 1199 (1976).
[14] C. Cohen-Tannoudji, in *Frontiers in Laser Spectroscopy*, edited by R. Balian, S. Haroche, and S. Liberman (North-Holland, Amsterdam, 1977), Vol. 1, pp. 3–104.
[15] S. Swain, J. Phys. B **8**, L437 (1975).
[16] H. J. Kimble and L. Mandel, Phys. Rev. A **13**, 2123 (1976).
[17] E. Courtens and A. Szöke, Phys. Rev. A **15**, 1588 (1977).
[18] B. Renaud, R. M. Whitley, and C. R. Stroud, Jr., J. Phys. B **10**, 19 (1970).
[19] P. L. Knight and P. W. Milonni, Phys. Rep. **66**, 21 (1980).
[20] Y. S. Bai, A. G. Yodh, and T. W. Mossberg, Phys. Rev. Lett. **55**, 1277 (1985).
[21] J. E. Golub and T. W. Mossberg, Phys. Rev. Lett. **59**, 2149 (1987).
[22] A. M. Bacon, H. Z. Zhao, L. J. Wang, and J. E. Thomas, Phys. Rev. Lett. **75**, 1296 (1995).
[23] H. Z. Zhao, Z. H. Lu, and J. E. Thomas, Phys. Rev. Lett. **79**, 613 (1997).
[24] H.-A. Bachor and D. E. McClelland, Phys. Scr. **T40**, 40 (1991).
[25] R. E. Slusher, L. W. Hollberg, B. Yurke, J. C. Mertz, and J. F. Valley, Phys. Rev. Lett. **55**, 2409 (1985).
[26] M. Maeda, P. Kumar, and J. H. Shapiro, J. Opt. Soc. Am. B **4**, 1501 (1987).

[27] L. A. Orozco, M. G. Raizen, M. Xiao, R. J. Brecha, and H. J. Kimble, J. Opt. Soc. Am. B **4**, 1490 (1987).
[28] M. Vallet, M. Pinard, and G. Grynberg, Europhys. Lett. **11**, 739 (1990).
[29] D. M. Hope, H.-A. Bachor, P. J. Manson, D. E. McClelland, and P. T. H. Fisk, Phys. Rev. A **46**, R1181 (1992).
[30] M. Kauranen, A. L. Gaeta, and R. W. Boyd, Opt. Commun. **103**, 211 (1993).
[31] M. Kauranen, A. L. Gaeta, R. W. Boyd, and G. S. Agarwal, Phys. Rev. A **50**, R929 (1994).
[32] W. V. Davis, M. Kauranen, E. M. Nagasako, R. J. Gehr, A. L. Gaeta, R. W. Boyd, and G. S. Agarwal, Phys. Rev. A **51**, 4152 (1995).
[33] J. P. Gordon and A. Ashkin, Phys. Rev. A **21**, 1606 (1980).
[34] J. Dalibard and C. Cohen-Tannoudji, J. Opt. Soc. Am. B **2**, 1707 (1985).
[35] M. J. Collett, D. F. Walls, and P. Zoller, Opt. Commun. **52**, 145 (1984).
[36] M. D. Reid and D. F. Walls, Phys. Rev. A **31**, 1622 (1985).
[37] A. Heidmann and S. Reynaud, J. Phys. (Paris) **46**, 1937 (1985).
[38] B. Wódkiewicz and J. H. Eberly, J. Opt. Soc. Am. B **2**, 458 (1985).
[39] For a recent review of optical noise, see S. Reynaud A. Heidmann, E. Giacobino, and C. Fabre, in *Progress in Quantum Optics XXX*, edited by E. Wolf (Elsevier, Amsterdam, 1992).
[40] S. E. Harris, Phys. Today **50**(7), 36 (1997).
[41] M. A. G. Martinez, P. R. Herczfeld, C. Samuels, L. M. Narducci, and C. H. Keitel, Phys. Rev. A **55**, 4483 (1997).
[42] F. I. Gauthey, C. H. Keitel, P. L. Knight, and A. Maquet, Phys. Rev. A **52**, 525 (1995).
[43] Janne Ruostekoski and D. F. Walls, Phys. Rev. A **55**, 3625 (1997).
[44] A. Aspect, G. Roger, S. Reynaud, J. Dalibard, and C. Cohen-Tannoudji, Phys. Rev. Lett. **45**, 617 (1980).
[45] C. A. Schrama, G. Nienhuis, H. A. Dijkerman, C. Steijsiger, and H. G. M. Heideman, Phys. Rev. Lett. **67**, 2443 (1991).
[46] K. D. Stokes, C. Schnurr, J. Gardner, M. Marable, S. Shaw, M. Goforth, D. E. Holmgren, and J. E. Thomas, Opt. Lett. **14**, 1324 (1989).
[47] C. Schnurr, K. D. Stokes, G. R. Welch, and J. E. Thomas, Opt. Lett. **15**, 1997 (1990).
[48] J. H. Shapiro, IEEE J. Quantum Electron. **QE-21**, 237 (1985).
[49] H. P. Yuen and V. W. S. Chan, Opt. Lett. **8**, 177 (1983).
[50] The method of squaring the spectrum analyzer output to obtain a signal which is linear in the power spectrum is well known in light beating spectroscopy. For an excellent review, see H. Z. Cummins and H. L. Swinney, in *Progress in Optics*, edited by E. Wolf (North-Holland, New York, 1970), Vol. VIII, Chap. 3, pp. 133–200.
[51] Similar methods have been used previously. See G. L. Abbas, V. W. S. Chan, and T. K. Yee, J. Lightwave Technol. **LT-3**, 1110 (1985).
[52] A. M. Bacon, H. Z. Zhao, L. J. Wang, and J. E. Thomas, Appl. Opt. **34**, 5326 (1995).
[53] Note that the phase of the LO in Ref. [35] is defined relative to the mean atomic dipole moment rather than with respect to the driving field, and so differs by 90° from our convention.
[54] Spectra similar to F_D and F_{SP} (without the Gaussian factor for the local oscillator) have been discussed in studies of fluorescence for two-level atoms driven by pulses short compared to the radiative lifetime. See K. Rzazewski and M. Florjanczyk, J. Phys. B **17**, L509 (1984); S. Cavalieri, R. Buffa, M. Matera, and M. Mazzoni, *ibid.* **20**, 5363 (1987); R. Buffa, S. Cavalieri, L. Fini, and M. Matera, *ibid.* **21**, 239 (1988); M. Lewenstein, J. Zakrzewski, and K. Rzazewski, J. Opt. Soc. Am. **3**, 22 (1986); T.-S. Ho and H. Rabitz, Phys. Rev. A **37**, 1576 (1988).
[55] E. J. Robinson and P. R. Berman, J. Phys. B **17**, L847 (1984).